Journal of Physics Communications

PAPER

Application of Grassmann phase space theory to Cooper pair model

N M Kidwani[1] and B J Dalton[1,2]

[1] Centre for Quantum and Optical Science, Swinburne University of Technology, Melbourne, Australia
[2] School of Physics and Astronomy, University of Glasgow, Glasgow, United Kingdom

E-mail: bdalton@swin.edu.au

OPEN ACCESS

RECEIVED
10 August 2019

ACCEPTED FOR PUBLICATION
4 November 2019

PUBLISHED
27 January 2020

Keywords: Grassmann phase space theory, Ito stochastic equations, Cooper pairs, numerical test

Abstract

This paper concerns the application of Grassmann phase space theory (GSPT) to treat the dynamical evolution of systems of identical fermions, such as ultracold gases of fermionic atoms. Phase space theory (which originated from quantum optics) is increasing in importance since it overcomes certain issues associated with other theoretical methods, such as Greens functions, variational methods, quantum-Monte-Carlo equations, etc. In phase-space theory quantum states are represented by quasi-probability distribution functions of phase space variables associated with canonical system operators—such as annihilation, creation operators. Evolution is described via a Fokker-Planck equation for the distribution function, which is equivalent to Ito stochastic equations for (time dependent) stochastic phase space variables. Quantum correlation functions given as averages of products of phase space variables over the quasi-probability distributions then become stochastic averages of products of stochastic phase space variables. In GSPT, the phase space variables are Grassmann numbers, but as computer representation of g-numbers is difficult, Grassmann phase space methods were regarded as being computationally inaccessible. However, previous work using the un-normalised B distribution shows that computer representation of Grassmann variables is unnecessary. Stochastic averages of products for quantum correlation functions at later times are related linearly to stochastic averages at earlier times via stochastic matrices only involving c-numbers. Thus, GSPT calculations of quantum correlation functions now only involve c-number computations. This paper presents the first correct numerical calculation of a quantum correlation function for a fermionic system using stochastic methods based on Grassmann phase space theory, namely the time dependence of the coherence between two Cooper pair states in a four-mode fermion system, where the short and finite time solutions can be compared to known exact results. Good agreement between the stochastic and exact results is found, showing that GPST is a valid approach for treating fermionic systems. The treatment of time evolution involves a novel use of the eigenvalues and biorthogonal column eigenvectors of a stochastically determined c-number matrix M and its transpose. Other topics of interest in ultra-cold fermi gases for which the GSPT could be applied are highlighted, such as the strong interaction regime for the BEC/BCS crossover achieved using magnetically tuned Feshbach resonance techniques.

1. Introduction

1.1. Theoretical methods for non-relativistic many-body systems

Quantum dynamics is one of the most fundamental problems in modern physics since time-evolution is the basis for any theoretical prediction, yet many-body complexity makes this an extremely challenging task in quantum systems. New theoretical methods are always needed, and quantitative experiments with well-understood interactions are vitally important to enable the testing of predictions. Also, for systems in thermodynamic equilibrium, evolution associated with changes to external variables such as temperature can also be thought of as a type of quantum dynamics. We will briefly review some of the recent developments

relevant to ultracold atoms since these provide an exceptionally simple and well-understood physical environment within which quantitative tests of dynamical theoretical predictions can be performed.

There is a wide range of theoretical treatments of the behaviour of many-body systems in non-relativistic quantum systems, which are found in condensed matter physics, nuclear physics, quantum optics and more recently in the physics of degenerate bosonic and fermionic atomic gases at low temperatures and density. These include not only the more traditional Green function [1, 2], variational [3, 4], path integrals [5], mean field theory [6] and stochastic Schrödinger equation-Quantum Monte Carlo [7] approaches, but also phase space methods [8–12]. In most modern treatments, where the many-body systems involve identical particles, a second quantisation approach [13, 14] is used.

There are well known issues regarding the theoretical methods described above. Path integrals and Monte-Carlo methods for instance, are useful for bosons at thermal equilibrium. However, for quantum dynamics and for fermions in particular, there are phase and sign problems, which severely limits their applicability. Also, the simulations involved are often restricted to small sizes which are difficult to extrapolate to the true thermodynamic limit [15–17]. The standard perturbation theory method, is applicable for certain problems, but others involving large interaction strengths may contain expansions which generally do not converge and are of infinite order due to a lack of a small expansion parameter. Using the mean field theory approach, one has to account for quantum fluctuations in atom numbers or limited coherence times and lengths [18]. Variational methods require an assumption regarding a trial function for which the choice depends on trial and error or experience. For Green functions, which have a long history in condensed matter problems—being applied to calculate properties of systems such as superfluids and superconductors [1, 19], a correct choice has to be made regarding the Feynman diagrams relevant to the problem.

Phase-space representations on the other hand, are of increasing importance as a viable and successful means to study exponentially complex quantum many-body systems from first principles [8–12]. These were invented to describe lasers, but have been adapted to treat atoms instead of photons. Consequently, the behaviour of bosonic photons and atoms is often treated using phase space methods in both quantum optics and cold atom physics. Here, mode annihilation and creation operators are represented by c-number phase space variables, with the density operator equivalent to a distribution function of these variables. Phase space methods have also been introduced for treating fermionic systems [20], but differing choices have been made for the phase space variables. Corney and Drummond [21] for example, introduce c-number variables associated with pairs of fermion annihilation, creation operators. However, the anti-commutation rules for fermion annihilation, creation operators suggests the possibility of using anti-commuting Grassmann variables to represent these operators [20]. However, in spite of the seminal work by Cahill and Glauber [20] (and a few other treatments [12, 22–27]), the use of Grassmann phase space methods in quantum—atom optics to treat fermionic systems is rather rare, though fermion coherent states using Grassmann variables are widely used in particle physics.

The present paper is the first correct numerical application of Grassmann phase space theory (GPST) to calculating a quantum correlation function (QCF) for a fermionic system (see section 1.2) for details). The QCF involved is the coherence between two Cooper pair states in a four mode fermionic system, showing the development of this coherence over finite times. This system has the advantage that the evolution is known via standard matrix mechanics, so although the GPST method is not expected to reveal any new physics in this case, it can be compared to a known exact result. New physics will be revealed when GPST is applied to systems not yet completely understood, such as the BEC/BCS crossover in cold Fermi gases. As will be shown below, (see sections 3.2, 3.3 for details) the evolution of the fermion QCF involves the stochastic calculation of a c-number matrix M, and a novel method for determining the evolution is presented, based on using the numerical eigenvalues and biorthogonal column eigenvectors of M and its transpose. Furthermore, the present paper clearly demonstrates that numerical calculations based on GPST can be carried out using only c-numbers, and without the need to represent Grassmann variables themselves on the computer –an issue previously thought to restrict GPST to purely analytic applications (see section 1.2 for details).

Unlike variational methods, phase space methods do not require assuming a trial form for the quantum state, and whereas Green function methods involve selecting which class of Feynman diagrams is important in the process and which are to be discarded, phase space methods do not depend on making such selections. They ultimately involve calculations with representative sets of stochastic trajectories that sample the distribution function throughout the phase space, and their main limitation is a numerical constraint on the numbers of trajectories that can be stored on a computer.

1.2. Phase space theory –Grassmann phase space variables

Thermal evolution based on a Matsubara equation [28] was treated using a Grassmann phase space theory by Plimak, Collett and Olsen [22] for a 1D system of spin 1/2 fermions with zero-range interactions, and numerical

results were presented for number correlations between pairs of fermions with various momentum, spin cases $(+\mathbf{k}\uparrow, -\mathbf{k}\downarrow, -\mathbf{k}\uparrow, +\mathbf{k}\downarrow)$. These authors used an un-normalized B distribution function based on fermion Bargmann coherent states [20] for which a Fokker-Planck equation (FPE) was obtained where the drift vector only depended linearly on the Grassmann phase space variables—a feature the authors recognised as being vital for numerical work. Plimak *et al* also introduced stochastic Grassmann variables, with those at a later time (or inverse temperature, for thermal evolution) being related linearly to those at an earlier time by a stochastic c-number transformation matrix β^{-1}. However, rather than introducing Ito SE for the stochastic variables themselves, they considered an Ito SE for the transformation matrix β. Their fundamental equation was an ansatz for determining the B distribution function at later times from that at an initial time, via substituting stochastic Grassmann variables for the original non-stochastic phase space variable, multiplying by the determinent ($det\ \beta$) of the transformation matrix, and then taking a stochastic average of the resultant product.

The Grassmann phase space theory used in the present paper was developed by Dalton *et al* on a different basis and is set out in [12, 24, 26] and [27]. Details are set out here in section 3. Extensive accounts of the underlying Grassmann algebra and calculus may be found in [12, 20, 22] and [25]. Essentially, the phase space method also involves representing the quantum density operator for the system by a Grassmann (un-normalized B) distribution function [12, 22, 24, 26, 27] and [25] in a phase space where the phase space variables replacing the fermion annihilation and creation operators are Grassmann variables. Quantum correlation functions (QCF) can be related to experimentally measurable quantities, and theoretically to Grassmann phase space integrals involving the distribution function with the fermion operators being replaced by phase space variables. Evolution equations (over time or temperature) for the density operator lead to Fokker-Planck equations (FPE) for the distribution function via the application of correspondence rules. However, unlike in [22], the FPE are then replaced by Ito stochastic equations for stochastic Grassmann phase space variables themselves, which are derived from the FPE. The QCF are now given by stochastic averages of products of these stochastic variables. The stochastic averages of products at a later time can be shown to be related linearly to such stochastic averages at an earlier time via matrices that only involve c-numbers. Even though these matrices involve stochastic quantities such as Wiener increments, their non-dependence on Grassmann variables enables computations to be carried out without having to represent Grassmann variables on the computer. The initial stochastic averages of products are obtained from the initial density operator. A comparison of the present approach with that in [22] is provided in the work of Polyakov [25], which confirmed the present formalism.

The utility of the theory can first be tested on some fermion systems that have been treated previously by other methods. In this paper, we will numerically calculate the coherence between two Cooper pair states in a simple four mode fermion system as a stochastic average [12, 24, 27]. The analytic short time and finite time solutions for such coherence are known using analytic methods, so comparisons can be made with exact results. Another test of the theory would involve a re-determination of the quantum correlation functions for interacting spin 1/2 fermions which were previously calculated by Plimak *et al* [20], by a Grassmann phase space approach involving a different treatment of evolution. Although based on a different Ito stochastic equation, the numerical calculations of Plimak *et al* [20], nevertheless showed that a Grassmann phase space theory could be used to calculate quantum correlation functions for a field-like situation involving a continuous range of momentum values –implying that similar calculations could be carried out on topics such as the BEC/BCS crossover.

1.3. Plan of paper

As the main potential application of Grassmann phase space theory will be to treat cold quantum gases of fermionic atoms, we provide in section 2 a brief overview of current topics of interest in this area. In section 3 we will review the various features of Grassmann Phase Space Theory starting with its key theoretical expressions, followed by how it can be used in numerical calculations. In section 4 we will describe the Cooper pair model for a system of two spin 1/2 fermions with four modes, comparing the theoretical results obtained for the model using analytical methods with the numerical results obtained for the QCF's based on GPST stochastic calculations. Section 5 summarises the paper. Various details are set out in Appendices, available as online Supplementary Material.

2. Cold quantum gases

Research in the field of ultracold atomic gases has been a major activity since the 1990's when Bose–Einstein condensation was achieved for bosonic atoms [29–32]. Non-interacting untrapped bosonic atoms at zero temperature form a BEC, with a macroscopic occupancy of the lowest single particle energy state, which is possible due to the absence of the Pauli exclusion principle. Since the 2000's ultracold gases of fermionic atoms have also been prepared manifesting different effects. Non-interacting untrapped fermionic atoms at zero

temperature form a Fermi gas, with each energy state only being occupied by two atoms with different spins due to the Pauli exclusion principle. Consequently, energy states are filled up to the Fermi energy E_F, whose associated wave number k_F is proportional to the inverse of the average separation between the atoms. In both cases, the single particle states are plane waves with momentum $\hbar k$.

Ultracold quantum gases have opened up new horizons in many-body physics, from novel quantum states of matter to quantum computing applications. They provide a unique table-top paradigm for exploring the properties of quantum many-body systems in nature, from the thermodynamics of high-temperature superconductors to the hydrodynamics of QCD Quark gluon plasmas (QGPs). These gases are mainly made of alkali metal atoms but also more recently other atoms as well as diatomic molecules. They can be fermionic or bosonic with a wide variety of internal hyperfine spin structures. They can be made strongly or weakly interacting, and both attractive and repulsive. They are contained in a variety of magnetic and optical traps in one, two and three dimensions, including optical lattices.

For bosonic gases, there is a wide range of interesting topics which include Bose–Einstein condensation (BEC) and superfluidity (flow without dissipation below a critical velocity v_c). The BEC paradigm, was first developed for non-interacting bosons, and later generalized to take into account repulsive interactions, describes bosonic fluids like ^{4}He or ultracold Bose gases like ^{87}Rb. Interactions are described in terms of a two-body scattering length [33]. The condensate is a macroscopic occupation of a single quantum state that occurs below a transition temperature T_c, which, even in strongly interacting Bose systems like ^{4}He, is of the same order of magnitude as the quantum degeneracy temperature at which the inter-particle spacing becomes of the order of the thermal de Broglie wavelength [34, 35].

For fermionic gases, not only do effects such as fermionic BCS superfluidity (based on large Cooper pairs of two atoms with opposite spins and momenta and described in terms of the BCS theory (Bardeen, Cooper Schrieffer [36])) occur, but also BEC superfluidity (based on tightly bound molecules of two fermionic atoms with opposite spins) can be observed. It was proposed as early as 1950 by Fritz London (see [37] that fermionic superfluidity for fermionic atoms is a pair condensate in momentum space, in contrast with a BEC of tightly bound pairs in real space, and BCS theory then emphasised the different nature of BCS and BEC types of suoperfluidity. The BCS paradigm, first developed for metallic superconductors, describes a pairing instability arising from a weak attractive interaction in a highly degenerate system of fermions. The formation of pairs, and their condensation, both occur at the same T_c that is orders of magnitude smaller than the Fermi energy E_F. However, it was later realised [38–41], that the BCS theory provided a good qualitative description of both the BEC and BCS regimes, as the two body scattering length is changed from being attactive (the BCS regime) to being negative (the BEC regime). Experimentally, such changes in the two body scattering length can be achieved using magnetically tuned Feshbach resonance [42–45] techniques. Studies involving Feshbach resonance have led to ground-breaking observations, including the condensation of molecules, and to additional intensive research relevant to the crossover physics, from a molecular Bose–Einstein condensate (BEC) to atomic Cooper pairs in the BCS state (BEC/BCS crossover) [17, 41, 46, 47]. The calculation of the phase transition temperature T_c between the superfluid phases as a function of $1/(k_F a)$ is also of interest. Near the crossover, the scattering length becomes very large, and this corresponds to the so-called unitary regime where strong correlations occur, and for which BCS theory involving mean field equations is no longer adequate. Figure 1 shows the phase diagram associated with a Feshbach resonance, the variables being the inverse of the two fermion scattering length and the temperature.

Various BEC/BCS crossover studies ([30, 48] -see figure 24) have shown that there is a smooth change in the size of the Cooper pairs through the Feshbach resonance. However, it is expected that there is little correlation between different Cooper pairs well away from the unitary regime. On the BEC side there should be little relationship between the nearby positions of the pair of fermions in one tightly bound molecular Cooper pair, and the positions of the pair of fermions in another. On the BCS side, there should be little relationship between the related k, $-k$ momenta of the pair of fermions in one Cooper pair and the related l, $-l$ momenta of the pair of fermions in another. However, in the crossover regime, the positions (or momenta) of the four fermions in any two Cooper pairs should be highly correlated. Figure 2 illustrates this effect.

A study of the BCS/BEC crossover regime—including the strong correlation unitary regime, would be a worthwhile application for Grassmann phase space theory. The application would employ Fokker-Planck equations and the related Ito stochastic equations either based on starting with a Matsubara equation [28], which describes the temperature evolution of the system from an initial high temperature where the atomic gas behaves classically, or starting with a Liouville-von Neumann equation, which describes time evolution. Numerical methods will be used at first to study the two particle quantum correlation function which has the form [49]:

$$\langle(\widehat{\psi}_\uparrow^\dagger(r_1)\widehat{\psi}_\downarrow^\dagger(r_2)\widehat{\psi}_\downarrow(r_2)\widehat{\psi}_\uparrow(r_1))\rangle. \tag{2.1}$$

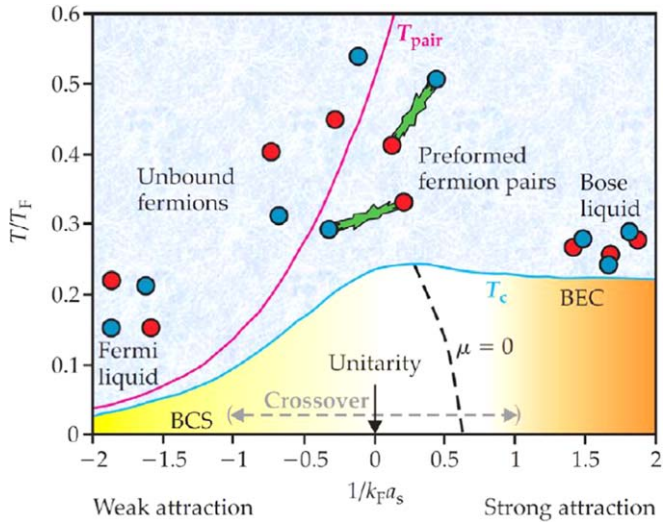

Figure 1. Ultracold Fermi gas phase diagram. Sketch of the BCS to BEC crossover for ultracold Fermi gases. When the scattering length as passes through a pole, so that $1/(k_F a_s) \to 0$, one obtains a strongly correlated fluid, the unitary gas. The critical temperature T_c for the phase transition only approaches the pairing temperature T_{pair} in the limit $1/(k_F a_s) \to -\infty$. The crossover region is the strongly interacting regime, loosely defined as $|1/(k_F a_s)| < 1$. Note that we denote the scattering length by a in the text [31]. Reproduced from Sá de Mello C A R 2008 Phys. Today 61 (10) 45, with the permission of the American Institute of Physics.

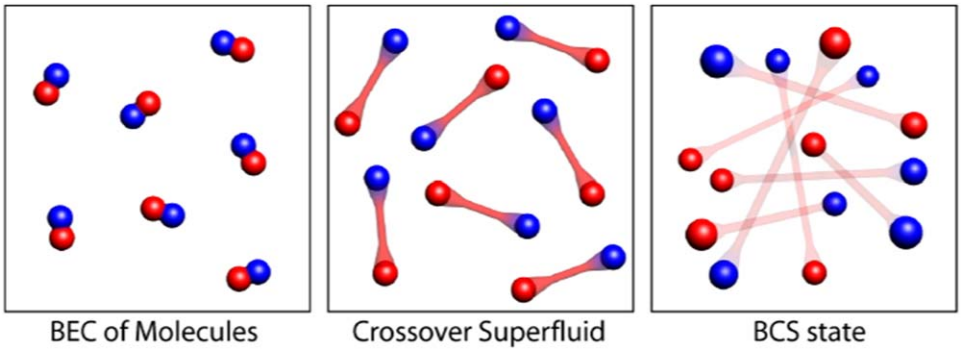

Figure 2. The BEC-BCS crossover. By tuning the interaction strength between the two fermionic spin states, one can smoothly cross over from a regime of tightly bound molecules to a regime of long-range Cooper pairs, whose characteristic size is much larger than the interparticle spacing. In between these two extremes, one encounters an intermediate regime where the pair size is comparable to the interparticle spacing interaction. Reprinted from Ketterle W and Zwierlein M W 2008 Ultracold Fermi Gases, Proc. of International School of Physics 'Enrico Fermi' ed M Inguscio et al (Amsterdam: IOS Press), with permission of IOS Press.

In the BCS theory, there is a smooth evolution in the BEC/BCS crossover in the size of the Cooper pair from the situation for a tightly bound molecule to that for a loosely bound Cooper pair with no dramatic change at resonance (see Ketterle [30]). It is expected that Grassmann phase space method would give similar results.

However, if higher order quantum correlations were studied, we might expect to see strong interaction effects, such as inter-pair coherence lengths differing from intra-pair coherence lengths, which are attributed to fluctuation correlations not included in the BCS mean field theory [48, 50–52]. Our hypothesis is that there is little correlation between different Cooper pairs well away from the unitary regime, however, in the crossover regime the positions of the four fermions in any two Cooper pairs should be highly correlated. As is well-known [49], the two particle QCF in equation (2.1) can be found using Bragg spectroscopy. However, the four particle QCF for describing one Cooper pair at r_1, r_2 and another at r_3, r_4 is

$$\langle \widehat{\Psi}^\dagger_\uparrow(\mathbf{r}_1)\widehat{\Psi}^\dagger_\downarrow(\mathbf{r}_2)\widehat{\Psi}^\dagger_\uparrow(\mathbf{r}_3)\widehat{\Psi}^\dagger_\downarrow(\mathbf{r}_4)\widehat{\Psi}_\downarrow(\mathbf{r}_4)\widehat{\Psi}_\uparrow(\mathbf{r}_3)\widehat{\Psi}_\downarrow(\mathbf{r}_2)\widehat{\Psi}_\uparrow(\mathbf{r}_1)\rangle. \tag{2.2}$$

This cannot be found using standard Bragg spectroscopy, suggesting that a new form of Bragg spectroscopy will be needed to fully study the strong interaction regime. On the theory side, the calculation of such QCF would be an important application of Grassmann phase space theory.

More recently, quantized vortices in a rotating Fermi gas have provided a direct signature for the presence of superfluidity in a strongly interacting Fermi gas, as they are a direct consequence of the existence of a

macroscopic wave-function that describes the superfluid. It is beyond the scope of this paper to describe these topics, but references such as [29, 30, 48, 50] provide a useful overview of the area.

Interacting fermions appear in a wide range of settings. The Grassmann phase space theory will be focused on applications to the specific topic of strongly interacting Fermi gases [30, 51], whichprovide a well-controlled and flexible environment to study many-body phenomena in strongly correlated systems. Generically, strong interactions give rise to strong correlations. A strongly correlated system cannot be described by working perturbatively from non-interacting particles or quasiparticles. In the case of electrons in condensed matter systems, theories constructed from single-particle properties, such as the Hartree–Fock approximation, cannot describe the problem at hand. In the case of fluids, the kinetic theories based on quasiparticle degrees of freedom, in particular the Boltzmann equation, fail [31, 53]. Theoretically, strongly interacting Fermi systems represent a challenging scenario to treat, as the large scattering length means there is no small parameter to describe the interactions. Models based on simple perturbation theory are therefore no longer adequate to describe certain system parameters. Experiments can provide useful information both revealing properties of these systems, and establishing benchmarks for appraising different approximate theoretical approaches. For example, recent experiments on ultracold Fermi gases have provided an unprecedented opportunity to test universality in the laboratory, which in principle allows for the interior properties of hot dense neutron stars to be investigated on earth [16].

3. Grassmann phase space theory

3.1. Summary of GPST features

As explained in section 1, in our work we follow the approach of Plimak, Collett and Olsen [23], in that we also base our work on the un-normalized B distribution, but with Grassmann number phase space variables (g_i, g_i^+) (rather than (g_i, g_i^*)) associated with each mode. Quantum correlation functions (QCF), Fock state populations and coherences are given by Grassmann phase space integrals over the B distribution function, with the mode operators being replaced by Grassmann phase space variables. Fokker-Planck equations for the distribution function are obtained, and these will involve Grassmann derivatives rather than c-number derivatives. The phase space variables are then replaced by stochastic Grassmann variables. The QCF, etc (as in the boson case) are now given by stochastic averages of products of the stochastic phase variables. However, unlike in [22], Ito stochastic equations for the stochastic Grassmann variables are derived from the Fokker-Planck equation. An approach for bosons described by Gardiner [54] is followed, where we equate the time derivative of the Grassmann phase space average of an arbitrary function of the phase space variables to the stochastic average of the same function when the Grassmann phase space variables are replaced by stochastic Grassmann variables. The time dependence of the phase space average is determined from the FPE for the distribution function and the time dependence of the stochastic average is determined from the Ito SE for the stochastic Grassmann variables, and these time dependences are required to be the same. This establishes the relationship between the deterministic and noise terms in the Ito SDE and the drift and diffusion terms in the FPE. It is a different approach to that based on the ansatz of Plimak *et al*, and our Grassmann Ito SE for the stochastic Grassmann variables are not equivalent to the c-number Ito SE for the transformation matrix obtained in [22]. A subsequent paper by Polyakov [25] was in agreement with our formalism.

We then show how the Ito SE for the stochastic Grassmann variables can be applied in numerical calculations of stochastic averages of products of these quantities needed for determining QCF, etc. Essentially, the stochastic average of a product of Grassmann stochastic phase variables at the end of a small time interval is related via a linear transformation to the set of stochastic averages of all the products of Grassmann stochastic phase variables (of the same order) at start of the time interval. The key result is showing that the linear transformation matrix M relating the stochastic Grassmann phase space variables at the end of a time interval to those at its beginning just involves c-numbers, such as stochastic Wiener increments and quantities from the Ito SE for the Grassmann stochastic phase variables. By dividing a finite time interval into small time intervals, the stochastic average of product of Grassmann stochastic phase variables at the end of the finite time interval can be obtained in steps from the stochastic averages of products of Grassmann stochastic phase variables at the initial time. The numerical method for this process involves calculating the eigenvalues and eigenvectors of the linear transformation matrix M and its transpose M^T for a suitably short time interval. Finally, the stochastic averages of products of Grassmann stochastic phase variables at the initial time are obtained from the initial density operator via expressions for QCF, Fock state populations and coherences, where the relevant phase space integrals are related to initial stochastic averages of products of Grassmann stochastic phase variables.

In order to treat problems involving large particle numbers, it is often convenient to consider field annihilation and creation operators rather than those for separate modes. A phase space theory based on fields can be constructed for fermions, as is the case for bosons. The density operator is represented by a Grassmann

distribution functional involving Grassmann fields associated with the field operators. The QCF etc are now given via Grassmann functional integrals. The distribution functional satisfies a functional Fokker- Planck equation (FFPE) involving Grassmann functional derivatives. Ito stochastic field equations (Ito SFE) can be obtained which are equivalent to the FFPE. The detailed development of Grassmann phase space field theory is covered in [12, 26, 27], but for reasons of space will not be outlined here.

In the next subsections we outline the separate mode treatment of Grassmann phase space theory.

3.2. Key theoretical expressions

3.2.1. Bargmann states

Fermion Bargmann coherent states are central to defining Grassmann phase space distribution functions. They are defined for a set of Grassmann numbers $g \equiv \{g_1, \ldots, g_i, \ldots, g_n\}$ for the modes $i = 1,2,..,n$ as

$$|g\rangle_B = \exp\left(\sum_i (\hat{c}_i^\dagger g_i)\right)|0\rangle = \prod_i (1 + \hat{c}_i^\dagger g_i)|0\rangle = \prod_i |g_i\rangle_B. \tag{3.1}$$

This is also an even Grassmann vector, but now only depends on g_i and not on the complex conjugates g_i^*. For the mode $|\varphi_i\rangle$ the Bargmann coherent state is

$$|g_i\rangle_B = (1 + \hat{c}_i^\dagger g_i)|0\rangle = |0_i\rangle - g_i|1_i\rangle, \tag{3.2}$$

which is a superposition of the vacuum state and a one-fermion state [12, 24, 26].

$|g_i\rangle_B$ only depends on g_i and not on g_i^*. The fermion Bargmann coherent state properties include the effect of the annihilation and creation operators $\hat{c}_i$ and $\hat{c}_i^\dagger$ for each mode i [12, 24, 26].

$$\begin{aligned}
\hat{c}_i\,|g\rangle_B &= g_i\,|g\rangle_B,\\
\hat{c}_i^\dagger\,|g\rangle_B &= \left(-\frac{\overrightarrow{\partial}}{\partial g_i}\right)|g\rangle_B,\\
\langle g^{+*}|_B\hat{c}_i &= \langle g^{+*}|_B\left(-\frac{\overleftarrow{\partial}}{\partial g_i^+}\right),\\
\langle g^{+*}|_B\hat{c}_i^\dagger &= \langle g^{+*}|_B g_i^+,
\end{aligned} \tag{3.3}$$

and they satisfy a completeness relation analogous to that for boson Bargmann coherent states, namely

$$\int\prod_i dg_i^* dg_i \exp(-g^*\cdot g)|g\rangle_B\langle g|_B = \hat{1}, \tag{3.4}$$

where $\mathbf{g}^*\cdot\mathbf{g} = \sum_i g_i^*\cdot g_i$.

3.2.2. Density operator and unnormalized B distribution function

The canonical form of the density operator in terms of fermion Bargmann states can also be written in terms of the unnormalized distribution function B as

$$\hat{\rho} = \int\prod_i dg_i^+ \prod_i dg_i B_{can}(g, g^+)|g\rangle_B\langle g^{+*}|_B, \tag{3.5}$$

where $\prod_i dg_i^+ = dg_1^+\cdot\cdots dg_n^+$ and $\prod_i dg_i = dg_n\cdots dg_1$- one should note that the Grassmann differentials anti-commute. Each fermion mode involves pairs of Grassmann phase space variables g_i, g_i^+. The canonical Grassmann phase space distribution function $B_{can}(g, g+)$ is obtained from Bargmann state matrix elements of the density operator and is given by

$$B_{can}(g, g^+) = \int\prod_i dg_i^{+*}\prod_i dg_i^*\langle g|_B\hat{\rho}\,|g^{+*}\rangle_B \times \exp(g\cdot g^* + g^{+*}\cdot g^+), \tag{3.6}$$

where $\prod_i dg_i^{+*} = dg_1^{+*}\cdot\cdots dg_n^{+*}$ and $\prod_i dg_i^* = dg_n^*\cdot\cdots dg_1^*$. The Grassmann distribution function $B(g, g^+)$ in equation (3.5) is unique, and is an even Grassmann function of $\{g_i, g_i^+\}$ of order 2^n [12, 22, 24].

The un-normalized $B(g, g^+)$ distribution function is related to the normalized distribution function $P(g, g^+)$ via [12, 24, 26]

$$B(g, g^+) = P(g, g^+)\exp(-\mathbf{g}\cdot\mathbf{g}^+). \tag{3.7}$$

The distribution function $P(g, g^+)$ is normalized to unity and could also be used to determine quantum correlation functions [12], though this would require directly solving the Fokker-Planck equations. However, in numerical calculations it is convenient to consider unnormalized forms of the distribution functions, as these turn out to result in simpler Fokker–Planck equations, and lead to Ito equations linear in the Grassmann variables—which can be treated numerically.

3.2.3. QCF, Fock state populations, coherences as phase space integrals

One set of important quantities that can be determined is that of the populations of, and coherences between, the fermion Fock states. We consider two Fock states –each with p occupied modes –given by

$$|\Phi\{l\}\rangle = (\hat{c}^{\dagger}_{l_1})(\hat{c}^{\dagger}_{l_2})..(\hat{c}^{\dagger}_{l_p})|0\rangle \qquad |\Phi\{m\}\rangle = (\hat{c}^{\dagger}_{m_1})(\hat{c}^{\dagger}{}_{m_2})..(\hat{c}^{\dagger}_{m_p})|0\rangle \tag{3.8}$$

Quantum correlation functions etc are given by Grassmann phase space integrals (see [12], pp.140–143).

$$Tr\{\hat{c}^{\dagger}_{l_1}...\hat{c}^{\dagger}_{l_p}\hat{\rho}\hat{c}_{m_q}...\hat{c}_{m_1}\} = \langle\hat{c}^{\dagger}_{l_1}...\hat{c}^{\dagger}_{l_p}\hat{c}_{m_q}...\hat{c}_{m_1}\rangle = \int\prod_i dg_i^+\prod_i dg_i g_{m_q}...g_{m_1}B(g,g^+)\times\exp(g\cdot g^+)g^+_{l_1}...g^+_{l_p}. \tag{3.9}$$

and for Fock states $|\Phi\{l\}\rangle$ and $|\Phi\{m\}\rangle$, the population and coherences are also phase space integrals given by

$$P(\Phi\{l\}) = \int\prod_i dg_i^+\prod_i dg_i g_{l_p}...g_{l_1}B(g,g^+)g^+_{l_1}...g^+_{l_p}. \tag{3.10}$$

$$C(\Phi\{m\};\Phi\{l\}) = \int\prod_i dg_i^+\prod_i dg_i g_{l_p}...g_{l_1}B(g,g^+)\times g^+_{m_1}...g^+_{m_p}. \tag{3.11}$$

3.2.4. Hamiltonian for cold quantum gases

The Hamiltonian for a fermion system involving one and two particle interactions, and may be written in terms of one particle and two particle operators $\hat{h}(a)$ and $\hat{V}(a,b) = \hat{V}(b,a)$

$$\hat{H}_f = \sum_a \hat{h}(a) + \frac{1}{2}\sum_{a,b}\hat{V}(a,b), \tag{3.12}$$

where the sums are over the N identical particles and the expressions are invariant under any permutation of these identical particles. In terms of annihilation and creation operators, the Hamiltonian given in first quantization by equation (3.12), can be written in the second quantization form

$$\hat{H}_f = \sum_{i,j} h_{ij}\hat{c}^{\dagger}_i\hat{c}_j + \frac{1}{2}\sum_{i,j,k,l} v_{ijkl}\hat{c}^{\dagger}_i\hat{c}^{\dagger}_j\hat{c}_l\hat{c}_k, \tag{3.13}$$

$$h_{ij} = \langle\phi_i(a)|\,\hat{h}(a)|\phi_j(a)\rangle, \tag{3.14}$$

$$v_{ijkl} = \langle\phi_i(a)|\langle\phi_j(b)|\,\hat{V}(a,b)|\phi_k(a)\rangle|\phi_l(b)\rangle. \tag{3.15}$$

The evolution of the quantum state allowing for both Hamiltonian dynamics and Markovian relaxation due to coupling to an external reservoir is described by a master equation [12, 24]

$$\frac{\partial}{\partial t}\hat{\rho} = \frac{1}{i\hbar}[\hat{H},\hat{\rho}] + \frac{1}{2}\sum_{a,b}\Gamma_{ab}(2\hat{S}^{\dagger}_b\hat{\rho}\hat{S}_a - \hat{\rho}\hat{S}_a\hat{S}^{\dagger}_b - \hat{S}_a\hat{S}^{\dagger}_b\hat{\rho}), \tag{3.16}$$

where for pairs fermion modes denoted $a \equiv i, j$ and $b \equiv k, l$ the transition operators $\hat{S}_a$ and relaxation coefficients Γ_{ab} are $\hat{S}_a = \hat{c}^{\dagger}_j\hat{c}_i$, $\hat{S}_b = \hat{c}^{\dagger}_l\hat{c}_k$ and $\Gamma_{ab} \equiv \Gamma_{ij;kl}$.

The symmetry features are

$$h_{ij} = h^*_{ji} \qquad v_{ijkl} = v_{jilk} = v^*_{klij} \qquad \Gamma_{ij;kl} = \Gamma^*_{kl;ij}. \tag{3.17}$$

3.2.5. Fokker-Planck equation—drift vector A and diffusion matrix D

Correspondence rules for replacing terms in the evolution equation for the density operator by equivalent terms in the Fokker-Planck equation for the B distribution function can be obtained using equation (3.3). These are set out as equation (45) in [24]. The Fokker-Planck equation for the B distribution function determines the dynamics in phase space and can be written using right Grassmann derivatives:

$$\frac{\partial}{\partial t}B(g,g^+) = -\sum_p^{2n}(A_pB(g,g^+))\frac{\overleftarrow{\partial}}{\partial g_p} + \frac{1}{2}\sum_{p,q=1}^{2n}(D_{pq}B(g,g^+))\frac{\overleftarrow{\partial}}{\partial g_q}\frac{\overleftarrow{\partial}}{\partial g_p}, \tag{3.18}$$

where $g_p \equiv g_1, \ldots, g_n, g^+_1, \ldots, g^+_n$.

3.2.6. Linearity of drift vector, bilinearity of diffusion matrix

The drift vector A is an odd Grassmann function, linearly dependent on the Grassmann variables. This key linearity feature is dependent on using the B distribution function and is vital for numerical work. The diffusion matrix D is even and is bilinearly dependent on the Grassmann variables. Unlike for bosons, it is an anti-symmetric matrix $D_{pq} = -D_{qp}$. For the Fokker-Planck equation equation (3.18), the drift vector A and the diffusion matrix D can be written in terms of submatrices (where T is the transpose).

$$[A] = \begin{bmatrix} \mathscr{C}^{-} \\ \mathscr{C}^{+} \end{bmatrix} \qquad [D] = \begin{bmatrix} -\mathscr{F}^{--} & +\mathscr{F}^{-+} \\ -(\mathscr{F}^{-+})^{T} & +\mathscr{F}^{++} \end{bmatrix}. \tag{3.19}$$

For the master equation equation (3.16), the quantities giving the drift vector in terms of the Hamiltonian matrix elements and relaxation coefficients are

$$\mathscr{C}_{i}^{-} = -\frac{1}{i\hbar}\sum_{j} h_{ij} g_{j} + \sum_{jk}\left(\frac{1}{2}\Gamma_{kikj}\right) g_{j}, \tag{3.20}$$

$$\mathscr{C}_{i}^{+} = \frac{1}{i\hbar}\sum_{j} h_{ij}^{*} g_{j}^{+} + \sum_{jk} g_{j}^{+}\left(\frac{1}{2}\Gamma_{kikj}^{*}\right), \tag{3.21}$$

where $\mathscr{C}_{i}^{-}$ and $\mathscr{C}_{i}^{+}$ are the submatrices of the drift vector A.

The quantities that define the sub-matrices submatrices $\mathscr{F}^{--}$, $\mathscr{F}^{+-}$, $\mathscr{F}^{-+}$,, $\mathscr{F}^{++}$, of the diffusion matrix D are

$$\mathscr{F}_{ij}^{--} = \sum_{kl}\left[\frac{1}{i\hbar}\upsilon_{ijkl} g_{l} g_{k} + \frac{1}{2}(\Gamma_{lijk} + \Gamma_{kjil}) g_{l} g_{k}\right] = -\mathscr{F}_{ji}^{--}, \tag{3.22}$$

$$\mathscr{F}_{ij}^{++} = \sum_{kl}\left[\frac{-1}{i\hbar}\upsilon_{ijkl}^{*} g_{k}^{+} g_{l}^{+} + \frac{1}{2}(\Gamma_{lijk}^{*} + \Gamma_{kjil}^{*}) g_{k}^{+} g_{l}^{+}\right] = -\mathscr{F}_{ji}^{++}, \tag{3.23}$$

$$\mathscr{F}_{ij}^{-+} = \sum_{kl}\Gamma_{jkil} g_{l} g_{k}^{+}, \quad \mathscr{F}_{ij}^{+-} = \sum_{kl}\Gamma_{jkil}^{*} g_{l}^{+} g_{k} = -\mathscr{F}_{ji}^{-+}. \tag{3.24}$$

In these submatrices $i, j = 1, 2, \ldots, n$ and the c-number quantities, Γ_{kikj}, ν_{ijkl} etc are defined in equations (3.14)–(3.17).

3.2.7. The stochastic and phase space averages

The Ito stochastic equations provide an equivalent determination of the phase space dynamics. As described in the Introduction, phase space variables g_{p} are replaced by time-dependent stochastic Grassmann variables $\tilde{g}_{p}(t)$. The *ith* member of the stochastic ensemble of $\tilde{g}_{p}(t)$ is denoted by $\tilde{g}_{i}^{p}(t)$, where $i = 1, \ldots, m$. For an arbitrary function $F(g, g^{+})$ of the Grassmann phase space variables, the phase space average $\langle F(g, g+)\rangle_{t}$ and the stochastic average $\overline{F(\tilde{g}(t), \tilde{g}^{+}(t))}$ of $F(g, g^{+})$ after the replacement by stochastic variables are given by

$$\overline{F(\tilde{g}(t), \tilde{g}^{+}(t))} = \frac{1}{m}\sum_{i=1}^{m} f(\tilde{g}_{pi}(t)), \tag{3.25}$$

$$\langle F(g, g^{+})\rangle_{t} = \iint dg^{+} dg F(g, g^{+}) B(g, g^{+}, t), \tag{3.26}$$

where for short $F(\tilde{g}(t), \tilde{g}^{+}(t))_{t} = f(\tilde{g}_{pi}(t))$

The stochastic equations for the $\tilde{g}_{p}(t)$ are determined from the Fokker-Planck equation for the distribution function $B(g, g^{+}, t)$ by requiring the phase space average of an arbitrary function $F(g, g^{+})$ and stochastic average of the same function to always coincide (see Gardiner, [54]). This will enable QCF, Fock state populations and coherence to either be given by a phase space integral involving the distribution function or a stochastic average involving the stochastic Grassmann phase space variables. Thus,

$$\langle F(g, g^{+})\rangle_{t} = \overline{F(\tilde{g}(t), \tilde{g}^{+}(t))}. \tag{3.27}$$

3.2.8. Ito equations for stochastic variables

The Ito stochastic equations for the stochastic Grassmann variables are given by

$$\frac{d}{dt}\tilde{g}_{p}(t) = C^{p}(\tilde{g}(t)) + \sum_{a} B_{a}^{p}(\tilde{g}(t))\Gamma_{a}(t_{+}), \tag{3.28}$$

where the deterministic term $C_{p}(\tilde{g}(t))$ and the noise factor $B_{a}^{p}(\tilde{g}(t))$ are odd Grassmann functions, and are yet to be determined. The $\Gamma_{a}(t_{+})$ are standard c-number Gaussian-Markov random noise terms These have the following stochastic properties

$$\overline{\Gamma_{a}(t_{1})} = 0 \qquad \overline{\Gamma_{a}(t_{1})\Gamma_{b}(t_{2})} = \delta_{ab}\delta(t_{1} - t_{2}), \tag{3.29}$$

$$\overline{\Gamma_{a}(t_{1})\Gamma_{b}(t_{2})\Gamma_{c}(t_{3})} = 0, \tag{3.30}$$

$$\overline{\Gamma_{a}(t_{1})\Gamma_{b}(t_{2})\Gamma_{c}(t_{3})\Gamma_{d}(t_{4})} = \overline{\Gamma_{a}(t_{1})\Gamma_{b}(t_{2})}\ \ \overline{\Gamma_{c}(t_{3})\Gamma_{d}(t_{4})} + \overline{\Gamma_{a}(t_{1})\Gamma_{c}(t_{3})}\ \ \overline{\Gamma_{b}(t_{2})\Gamma_{d}(t_{4})} + \overline{\Gamma_{a}(t_{1})\Gamma_{d}(t_{4})}\ \ \overline{\Gamma_{b}(t_{2})\Gamma_{c}(t_{3})}, \tag{3.31}$$

with the stochastic average of any odd number product being zero, and that for any even number product being determined from sums of products of the $\overline{\Gamma_{a}(t_{1})\Gamma_{b}(t_{2})}$. More explicitly equations (3.29), (3.30) and (3.31) show

that the stochastic averages of a single Γ is zero and the stochastic average of the product of two Γ 's is zero if they are different, and delta function correlated in the time difference if they are the same. In addition, the stochastic averages of products of odd numbers of Γ are zero, and stochastic averages of products of even numbers of Γ are the sums of products of stochastic averages of pairs of Γ. At this stage, we just list the Γ_a via $a = 1,2,\ldots,i(n)$, where the total number $i(n)$ is expected to depend on the number of modes n. It will turn out that $i(n) = 2n^2$.

3.2.9. The Uncorrelation property

An additional property is that any $F(\tilde{g}(t))$ and the products of any $\Gamma_a(t_+)$ at later times t_+ are *uncorrelated.*

$$\overline{F(\tilde{g}(t_1))\Gamma_a(t_2)\Gamma_b(t_3)\Gamma_c(t_4)\cdot\cdot\Gamma_k(t_l)} = \overline{F(\tilde{g}(t_1))} \times \overline{\Gamma_a(t_2)\Gamma_b(t_3)\Gamma_c(t_4)\cdot\cdot\Gamma_k(t_l)}, \tag{3.32}$$

where $t_1 < t_2, t_3, \ldots, t_l$.

3.2.10. The integral form of the Ito equation –the Wiener increments

Together with the stochastic averaging properties, the uncorrelation property and stochastic properties of sums and products, an expression for the time derivative of the stochastic average of $F(\tilde{g}, \tilde{g}^+)$ can be derived, which involves the $C_p(\tilde{g}(t))$ and $B_a^p(\tilde{g}(t))$ Grassmann functions in the Ito stochastic equations. The Ito stochastic equation for $\tilde{g}_p(t)$ can also be written in the integral form

$$\delta\tilde{g}_p(t) = C^p(\tilde{g}_q(t))\delta t + \sum_a B_a^p(\tilde{g}_q(t))\delta\tilde{\omega}_a(t_+), \tag{3.33}$$

where

$$\delta\tilde{g}_p(t) = \tilde{g}_p(t+\delta t) - \tilde{g}_p(t), \tag{3.34}$$

is a Grassmann stochastic increment, and the Wiener stochastic variable $\tilde{\omega}_a$ and Wiener increment are

$$\tilde{\omega}_a(t) = \int_{t_0}^{t} dt_1\Gamma_a(t_1) \qquad \delta\tilde{\omega}_a(t_+) = \int_{t+}^{t+\delta t} dt_1\Gamma_a(t_1). \tag{3.35}$$

An important result for the stochastic average of the product of two Wiener increments is

$$\overline{\delta\tilde{\omega}_a(t_+)\delta\tilde{\omega}_b(t_+)} = \delta_{a,b}\delta t, \tag{3.36}$$

which can easily be derived using equations (3.35) and (3.29).

The following results for stochastic averages of products of Wiener increments can also be obtained,

$$\overline{\delta\tilde{\omega}_a(t_i)} = 0 \qquad \overline{\delta\tilde{\omega}_a(t_i)\delta\tilde{\omega}_b(t_j)} = \delta_{a,b}\delta_{ij}(\delta t), \tag{3.37}$$

$$\overline{\delta\tilde{\omega}_a(t_i)\delta\tilde{\omega}_b(t_j)\delta\tilde{\omega}_c(t_k)} = 0, \tag{3.38}$$

$$\begin{aligned}\overline{\delta\tilde{\omega}_a(t_i)\delta\tilde{\omega}_b(t_j)\delta\tilde{\omega}_c(t_k)\delta\tilde{\omega}_d(t_l)} &= \overline{\delta\tilde{\omega}_a(t_i)\delta\tilde{\omega}_b(t_j)}\ \ \overline{\delta\tilde{\omega}_c(t_k)\delta\tilde{\omega}_d(t_l)} + \overline{\delta\tilde{\omega}_a(t_i)\delta\tilde{\omega}_c(t_k)}\ \ \overline{\delta\tilde{\omega}_b(t_j)\delta\tilde{\omega}_d(t_l)} \\ &+ \overline{\delta\tilde{\omega}_a(t_i)\delta\tilde{\omega}_d(t_l)}\ \ \overline{\delta\tilde{\omega}_b(t_j)\delta\tilde{\omega}_c(t_k)} \\ &= \{\delta_{ab}\delta_{ij}\delta_{cd}\delta_{kl} + \delta_{ac}\delta_{ik}\delta_{bd}\delta_{jl} + \delta_{ad}\delta_{il}\delta_{bc}\delta_{jk}\}(\delta t)^2.\end{aligned} \tag{3.39}$$

3.2.11. Relation between FPE and Ito equations' quantities

By equating the time derivatives of the two averages in equations (3.25) and (3.26) for an arbitrary function $F(g, g^+)$, the following important relationships between A and D in FPE, and C and B occurring in Ito SE are found.

$$C^p(g, g^+) = -A_p(g, g^+), \tag{3.40}$$

$$[B(g, g^+)B^T(g, g^+)]_{qp} = D_{qp}(g, g^+). \tag{3.41}$$

The detailed derivation is set out in [12].

The deterministic factor C in the Ito SE is easily obtained as the negative of the drift vector A in the FPE (the opposite sign to the boson case). As for bosons, the noise factor B is related to the diffusion matrix D in the FPE via $BB^T = D$, but now with $D^T = -D$. It is obtained via a construction process involving Takagi factorization [55, 56].

From the bilinearity of the diffusion matrix elements we can write (see appendix A, equation (A.4))

$$D_{pq} = \sum_{r,s=1}^{2n} Q_{rs}^{pq} g_r g_s, \tag{3.42}$$

where Q is a $2n^2 \times 2n^2$ complex and symmetric matrix (from $D_{pq} = -D_{qp}$) of c-numbers. The rows $\{p, r\}$ and columns $\{q, s\}$ of Q are listed as $1, \ldots, 2n^2$. Using Takagi factorization [55, 56]- with the columns of K listed as $a = 1, \ldots, 2n^2$ we can write

$$Q = K(K)^T \qquad Q_{rs}^{pq} = \sum_a K_{r,a}^p K_{s,a}^q. \tag{3.43}$$

We choose $B_a^p(g)$ in terms of c-numbers $K_{r,a}^p$ as a linear function of the Grassmann phase space variables

$$B_a^p(g, g^+) = \sum_{r=1}^{2n} K_{r,a}^p g_r. \tag{3.44}$$

It is then easily shown that $(BB^T)_{pq} = D_{pq}$, which solves the equation for the noise factor B.

Hence, we have now found a matrix B such that $BB^T = D$. As there are $2n^2$ columns for K, it follows that the number of Gaussian–Markov or Wiener stochastic variables in the Ito equations is $2n^2$ also. This contrasts to the smaller number $2n$ for the boson case.

From the linearity of the drift vector elements we can write it in the form (see appendix A, equation (A.7)).

$$A_p(g) = -\sum_r L_r^p g_r, \tag{3.45}$$

where L is a $2n \times 2n$ matrix of c-numbers, with rows p and columns r which are listed as $1, 2 \ldots, 2n$.

Hence, we have from equation (3.40)

$$C^p(g, g^+) = \sum_{r=1}^{2n} L_r^p g_r. \tag{3.46}$$

3.2.12. Linear relation for Grassmann stochastic variables –The Θ matrix

By combining the results in equations (3.44), (3.46) for $B_a^p(g)$ and $C_p(g)$, the Ito stochastic equations can now be written

$$\begin{aligned} \tilde{g}_p(t + \delta t) &= \textstyle\sum_r \left\{ \delta_{p,r} + L_r^p \delta t + \sum_a K_{r,a}^p \delta\tilde{\omega}_a(t_+) \right\} \tilde{g}_r(t) \\ &= \textstyle\sum_r \Theta_{p,r}(t^+) \tilde{g}_r(t), \end{aligned} \tag{3.47}$$

where the Wiener increment is $\delta\tilde{\omega}_a(t_+) = \int_{t+}^{t+\delta t} dt_1 \Gamma_a(t_1)$. Note there are $2n^2$ increments. The quantity in brackets $\Theta_{p,r}(t +)$ only involves c-numbers, and equation (3.47) shows there is a linear relationship involving a c-number stochastic transformation matrix between the Grassmann stochastic phase space variables at time t and those at time $t + \delta t$. If the evolution between t_0 and $t_f = t_{n+1}$ is divided into small intervals $t_i \to t_{i+1}$ with $i = 0, \ldots, n$ then

$$\begin{aligned} \tilde{g}_p(t_f) &= \textstyle\sum_{r,s,\ldots..z} \Theta_{p,r}(t_n^+) \Theta_{r,s}(t_{n-1}^+) \ldots \Theta_{y,z}(t_0^+) \tilde{g}_z(t_0) \\ &= \textstyle\sum_z \Lambda_{p,z}(t_f, t_0) \tilde{g}_z(t_0). \end{aligned} \tag{3.48}$$

This shows that the stochastic Grassmann variables at final time depend linearly on the SGV at earlier time via a stochastic transformation matrix that involves only c-numbers. A similar feature applies in Plimak Collett and Olsen [22]. This linearity feature is only present for the B distribution. For the P distribution the drift vector $C^p(g)$ involves terms that depend cubically on the Grassmann variables. Although the P distribution function is still equivalent to Ito stochastic equations, the third order feature of the drift vector results in the Ito equations not being of use in numerical calculations [22, 24]. However, the P distribution function and its equivalent Ito stochastic equations are still useful for formal theory.

The number of stochastic c-number Wiener increments involved is $2n^2$, which increases as square of number of modes. A similar number of increments applies in the Gaussian phase-space treatment developed by Corney and Drummond [21].

3.2.13. QCFs, populations and coherences as stochastic averages

The QCF, Fock state populations, coherences are now given by stochastic average of product of stochastic Grassmann variables instead of phase space integrals. Thus

$$P(\Phi\{l\})_t = \overline{(\tilde{g}_{l_p}(t) \ldots \tilde{g}_{l_1}(t))(\tilde{g}_{l_1}^+(t) \ldots \tilde{g}_{l_p}^+(t))}, \tag{3.49}$$

$$C(\Phi\{m\}; \Phi\{l\})_t = \overline{(\tilde{g}_{l_p}(t) \ldots \tilde{g}_{l_1}(t))(\tilde{g}_{m_1}^+(t) \ldots \tilde{g}_{m_p}^+(t))}, \tag{3.50}$$

$$Tr\{(\hat{c}_{l_1}^\dagger)(\hat{c}_{l_2}^\dagger) \ldots (\hat{c}_{l_p}^\dagger) \hat{\rho} (\hat{c}_{m_q}) \ldots (\hat{c}_{m_2})(\hat{c}_{m_1})\} = \overline{(\tilde{g}_{m_q}) \ldots (\tilde{g}_{m_1}) \exp(\tilde{g} \cdot \tilde{g}^+)(\tilde{g}_{l_1}^+) \ldots \tilde{g}_{l_p}^+)}. \tag{3.51}$$

3.2.14. General equations of QCFs –Stochastic evolution of QCF, populations and coherences

By dividing the evolution between t_0 and $t_f = t_{n+1}$ into equal small intervals with $t_{i+1} = t_i + \delta t$ with $i = 0, \ldots, n$, then using equation (3.47) in each factor for a product of the stochastic Grassmann variables at time $t_i + \delta t$, we can then place all the stochastic Grassmann variables for time t_i together in order and finally take the stochastic average of both sides to obtain the result

$$\overline{\widetilde{g}_p(t_i+\delta t)\widetilde{g}_q(t_i+\delta t)\ldots\widetilde{g}_s(t_i+\delta t)} = \sum_{x,y,\ldots u}[\Theta_{p,x}(t_i^+)\Theta_{q,y}(t_i^+)\ldots\Theta_{s,u}(t_i^+)]_{Stochastic\ Avg} \times \overline{\widetilde{g}_x(t_i)\widetilde{g}_y(t_i)\ldots\widetilde{g}_u(t_i)}, \tag{3.52}$$

where the uncorrelation property equation (3.32) - has been used. This shows that the stochastic average of products of $\widetilde{g}(t_i + \delta t)$ at time $t_i + \delta t$ given by sums over stochastic averages of products of the c-number stochastic quantities in the square bracket in equation (3.52) times stochastic averages of the various products of $\widetilde{g}_z(t_i)$ at time t_i. The numbers of factors in such products of stochastic Grassmann variables is the same for times t_i and t_{i+1}. This enables a set of stochastic averages of products of Grassmann stochastic variables of a given order to be propagated over a number of small intervals in succession from an initial time to a final time. The c-number quantities in the square bracket involve Wiener increments and quantities determined from the FPE using equations (3.40), (3.41), (3.42), (3.43), (3.44) and (3.46). The stochastic averages of products of the $\widetilde{g}_z(t_0)$ at the initial timet_0 are determined from initial density operator at time t_0 using equation (3.51) (see [27], equation (25)).

Thus, numerical calculations for the dynamical and thermal evolution of the QCF, Fock state populations and coherences can be carried out without having to represent the Grassmann variables themselves on a computer.

3.3. General numerical method

3.3.1. X vector for QCF of given order –Constructing the matrices $X_{(t)}$, $M_{\alpha,\beta}$ and $X_{(t+\delta t)}$ for the general case

We can list the distinct $\widetilde{g}_p\widetilde{g}_q\ldots\widetilde{g}_s$ and $\widetilde{g}_x\widetilde{g}_y\ldots\widetilde{g}_u$ occuring in equation (3.52) in a standard order $\widetilde{g}_n\widetilde{g}_{n-1}\ldots\widetilde{g}_1\widetilde{g}_1^+\widetilde{g}_2^+\ldots\widetilde{g}_n^+$.

The distinct $\overline{\widetilde{g}_p(t+\delta t)\widetilde{g}_q(t+\delta t)\ldots\widetilde{g}_s(t+\delta t)}$ and $\overline{\widetilde{g}_x(t)\widetilde{g}_y(t)\ldots\widetilde{g}_u(t)}$ become elements $X_1, X_2, .., X_N$ of column vectors , so equation (3.52) involves matrix multiplication.

The result is

$$\begin{bmatrix} X_1 \\ X_2 \\ . \\ X_N \end{bmatrix}_{t+\delta t} = \begin{bmatrix} M_{1,1} & M_{1,2} & .. & M_{1,N} \\ M_{2,1} & M_{2,2} & .. & M_{2,N} \\ .. & .. & .. & .. \\ M_{N,1} & M_{N,2} & .. & M_{N,N} \end{bmatrix}_{t+t_+} \begin{bmatrix} X_1 \\ X_2 \\ . \\ X_N \end{bmatrix}_t . \tag{3.53}$$

3.3.2. M matrix and stochastic average of sums of products of theta matrices, permutation factors

The matrix elements $M_{\{p,q,..,s\};\{x,y,..,u\}}$ are given in terms of stochastic average of products of Θ elements

$$M_{\{p,q,..,s\};\{x,y,..,u\}}(t_+) = \sum_P \overline{\Theta_{p,\mu_x}(t^+)\Theta_{q,\mu_y}(t^+)\ldots\Theta_{s,\mu_u}(t^+)} \times (-1)^P \tag{3.54}$$

where $P = (x \to \mu_x,\ y \to \mu_y\ ,..,\ u \to \mu_u)$ are permutations of $x,\ y,\ ..,\ u$ from the standard order $\{x,\ y,\ ..,\ u\}$, and $(-1)^P = +1,\ -1$ if permutation P of $x,\ y,\ ..,\ u$ is even, odd.

3.3.3. Equations for QCF in terms of M matrix

We can divide the evolution between t_0 and $t_f = t_{n+1}$ into small intervals $t_i \to t_{i+1}$ with $i = 0,\ ..,\ n$ so that

$$\overrightarrow{X}(t_f) = M(t_n^+) \times M(t_{n-1}^+) \times \ldots M(t_0^+) \times \overrightarrow{X}(t_0) \tag{3.55}$$

The vector $\overrightarrow{X}(t_f)$ listing the stochastic averages of distinct products of $\widetilde{h}_p(t_f)$ at time t_f is given by successively applying matrix multiplication by M matrices to vector $\overrightarrow{X}(t_0)$ listing products of $\widetilde{g}_z(t_0)$ at time t_0 —same numbers as for $\widetilde{g}_p(t_f)$. The stochastic averages for $\overrightarrow{X}(t_0)$ are determined from the initial density operator at time t_0.

Hence no computer representation of Grassmann variables is involved, thus enabling numerical calculations for dynamical and thermal evolution.

If the time increments are equal to δt and the M matrices are the same, then equation (3.55) simplifies to

$$\overrightarrow{X}(t_f) = (M(\delta t))^n \times \overrightarrow{X}(t_0) \tag{3.56}$$

3.3.4. Expression for M matrix in terms of eigenvalues and eigenvectors of M and M^T

Let ξ_μ be the eigenvector of M with eigenvalue μ

$$M\xi_\mu = \mu\xi_\mu. \tag{3.57}$$

where the ξ_μ are normalized $\xi_\mu^T\xi_\mu = 1$, where T is the transpose operation.

Let η_ν be the column eigenvector of M^T with eigenvalue ν

$$M^T\eta_\nu = \nu\eta_\nu. \tag{3.58}$$

The eigenvalues of M, M^T are the same ($|M^T - \nu I| = |M - \nu I|$)

A little algebra will lead to

$$\mu(\eta_\mu^T\xi_\nu) = \nu(\eta_\mu^T\xi_\nu),$$

which if $\mu \neq \nu$ could only be true if $\eta_\mu^T\xi_\nu = 0$. Thus

$$(\eta_\mu^T\xi_\nu) = \delta_{\mu,\nu}. \tag{3.59}$$

so the η_μ, ξ_μ form biorthogonal set. We have chosen the norm of η_μ such that $\eta_\mu^T\xi_\mu = 1$.

Assuming that the eigenvectors ξ_ν are linearly independent, one can then show that

$$M = \sum_\mu \mu\xi_\mu\eta_\mu^T, \tag{3.60}$$

3.3.5. Time evolution of QCFs in terms of eigenvalues and eigenvectors of M and M^T–Expressions for powers of M

The square of M is given by

$$\begin{aligned} M^2 &= \textstyle\sum_\mu\sum_\nu \mu\xi_\mu\eta_\mu^T\nu\xi_\nu\eta_\nu^T = \sum_{\mu\nu}\mu\nu\xi_\mu\eta_\nu^T(\eta_\mu^T\xi_\nu) \\ &= \textstyle\sum_\mu \mu^2\xi_\mu\eta_\mu^T, \end{aligned} \tag{3.61}$$

where we have used the orthogonality relation of equation (3.59) and $\eta_\nu^T\xi_\nu = 1$.

Generalizing the result of equation (3.61) we have

$$M^n = \sum_\mu \mu^n\xi_\mu\eta_\mu^T. \tag{3.62}$$

Since the Θ matrices equal the unit matrix plus a correction of order δt, the eigenvalues of M may be written to a good approximation as

$$\mu = r_\mu e^{ia_\mu\delta T}, \tag{3.63}$$

we see that

$$M^n = \sum_\mu e^{ia_\mu n\delta T}\xi_\mu\eta_\mu^T(r_\mu)^n = \sum_\mu e^{ia_\mu T}\xi_\mu\eta_\mu^T(r_\mu)^{\frac{T}{\delta T}}, \tag{3.64}$$

where $T = n\delta T$. For small δT, $a_\mu \sim 1$ and $r_\mu \doteqdot 1$. This expression can be used in conjunction with equation (3.56) to determine the time evolution of the coherences and populations. In Eqs. (3.63) and (3.64) we have written the time interval $(t_f - t_0)$ and the time increment δt in suitable dimensionless units as T and δT (see section 4.2.1).

3.3.6. Case of symmetric M

In the case where M is symmetric the eigenvectors of M and M^T are the same $\xi_\mu = \eta_\mu$ and we now have the simplified expressions

$$\begin{aligned} M &= \sum_\mu e^{ia_\mu\delta T}\xi_\mu\xi_\mu^T(r_\mu) \\ M^n &= \sum_\mu e^{ia_\mu T}\xi_\mu\xi_\mu^T(r_\mu)^{\frac{T}{\delta T}}. \end{aligned} \tag{3.65}$$

These expressions will be used to determine the finite time evolution of the coherence based on the analytic form of the M matrix.

4. Cooper pair model

4.1. System of two spin $\frac{1}{2}$ fermions

Here, we will treat a simple four mode problem involving two spin 1/2 fermions in free space in order to test Grassmann phase space theory numerically. For this case we can obtain analytic results to compare with. We will

consider the dynamical evolution of coherences between two distinct Cooper pair states in the situation where the system is initially in one of these states, and where relaxation processes and external potentials are ignored. A non-numerical initial treatment of how the two-fermion-number correlations develop, owing to coupling between the two distinct Cooper pair states via the short-range interatomic interactions, is set out in [12, 24, 27].

4.1.1. Modes

The four modes involved are [12, 24, 27].

$$|\phi_1\rangle = |\phi_{\mathbf{k},+}\rangle \qquad |\phi_2\rangle = |\phi_{\mathbf{k},-}\rangle,$$
$$|\phi_3\rangle = |\phi_{-\mathbf{k},+}\rangle \qquad |\phi_4\rangle = |\phi_{-\mathbf{k},-}\rangle, \tag{4.1}$$

with momenta $-\mathbf{k}$, $+\mathbf{k}$, spin components $-,+$ and energies ω. Their spatial mode functions are given by

$$\phi_1(\mathbf{r}) = (\langle +|\langle \mathbf{r}|)|\phi_1\rangle = \frac{1}{\sqrt{V}}\exp(i\mathbf{k}\cdot\mathbf{r}) \qquad \phi_2(\mathbf{r}) = (\langle -|\langle \mathbf{r}|)|\phi_2\rangle = \frac{1}{\sqrt{V}}\exp(i\mathbf{k}\cdot\mathbf{r}),$$
$$\phi_3(\mathbf{r}) = (\langle +|\langle \mathbf{r}|)|\phi_3\rangle = \frac{1}{\sqrt{V}}\exp(-i\mathbf{k}\cdot\mathbf{r}) \qquad \phi_4(\mathbf{r}) = (\langle -|\langle \mathbf{r}|)|\phi_4\rangle = \frac{1}{\sqrt{V}}\exp(-i\mathbf{k}\cdot\mathbf{r}), \tag{4.2}$$

where the mode functions are box normalized in a volume $V = L^3$.

The mode annihilation operators are denoted

$$\hat{c}_{k\uparrow} = \hat{c}_1, \qquad \hat{c}_{k\downarrow} = \hat{c}_2, \qquad \hat{c}_{-k\uparrow} = \hat{c}_3, \qquad \hat{c}_{-k\downarrow} = \hat{c}_4. \tag{4.3}$$

Allowing for only the above four modes the field operators for spin $+$ and spin $-$ fermions are

$$\hat{\Psi}_+(\mathbf{r}) = \hat{c}_1\phi_1(\mathbf{r}) + \hat{c}_3\phi_3(\mathbf{r}) \qquad \hat{\Psi}_-(\mathbf{r}) = \hat{c}_2\phi_2(\mathbf{r}) + \hat{c}_4\phi_4(\mathbf{r}). \tag{4.4}$$

4.1.2. Hamiltonian

Hamiltonian dynamics will be considered based on equation (3.13), with coupling constant g describing the interaction terms In first quantization the interaction between the fermions is given by

$$\hat{V} = \frac{g}{2}\sum_{\substack{i,j\\ \alpha}} \delta_{\alpha i,\bar{\alpha} j}\delta(\mathbf{r}_i - \mathbf{r}_j), \tag{4.5}$$

where $\mathbf{r}$ denotes space and α denotes spin ($\uparrow$, $\downarrow$). $\overline{\alpha}$ denotes the opposite spin to α. The free fermion kinetic energy is given by

$$\hat{T} = \frac{1}{2M}\sum_{i\alpha}\hat{\mathbf{p}}_{i\alpha}^2. \tag{4.6}$$

Using the notation in equation (4.3) the Hamiltonian can be written in second quantization

$$\hat{H} = \hat{H}_0 + \hat{H}_1, \tag{4.7}$$

as the sum of one-fermion and two-fermion terms where

$$\hat{H}_0 = \hbar\omega(\hat{c}_1^\dagger\hat{c}_1 + \hat{c}_2^\dagger\hat{c}_2 + \hat{c}_3^\dagger\hat{c}_3 + \hat{c}_4^\dagger\hat{c}_4), \tag{4.8}$$

$$\hat{H}_1 = \frac{g}{2V}(\hat{c}_1^\dagger\hat{c}_2^\dagger\hat{c}_2\hat{c}_1 + \hat{c}_2^\dagger\hat{c}_1^\dagger\hat{c}_1\hat{c}_2 + \hat{c}_1^\dagger\hat{c}_4^\dagger\hat{c}_4\hat{c}_1 + \hat{c}_4^\dagger\hat{c}_1^\dagger\hat{c}_1\hat{c}_4 + \hat{c}_3^\dagger\hat{c}_2^\dagger\hat{c}_2\hat{c}_3 + \hat{c}_2^\dagger\hat{c}_3^\dagger\hat{c}_3\hat{c}_2 + \hat{c}_3^\dagger\hat{c}_4^\dagger\hat{c}_4\hat{c}_3 + \hat{c}_4^\dagger\hat{c}_3^\dagger\hat{c}_3\hat{c}_4$$
$$+ \hat{c}_1^\dagger\hat{c}_4^\dagger\hat{c}_2\hat{c}_3 + \hat{c}_4^\dagger\hat{c}_1^\dagger\hat{c}_3\hat{c}_2 + \hat{c}_3^\dagger\hat{c}_2^\dagger\hat{c}_4\hat{c}_1 + \hat{c}_2^\dagger\hat{c}_3^\dagger\hat{c}_1\hat{c}_4), \tag{4.9}$$

and $\hbar\omega = \hbar^2k^2/2M$. Expressions for h_{ij} and ν_{ijkl} are obtained using equations (3.14), (3.15) above. As the spatial mode functions are plane waves, normalised in a box V, consequently periodic boundary conditions based on equation (4.2) result in many terms being zero and many terms being equal. The one-body terms are diagonal and all equal. Several of the two-body terms are zero and the remainder are equal.. In terms of the general notation in equations (3.14), (3.15), the non-zero h_{ij} and ν_{ijkl} are

$$h_{11} = h_{22} = h_{33} = h_{44} = \hbar\omega, \tag{4.10}$$

and

$$h_{12} = h_{13} = h_{14} = h_{23} = h_{24} = h_{34} = 0, \tag{4.11}$$

$$\nu_{1212} = \nu_{2121} = \nu_{1414} = \nu_{4141} = \nu_{3232} = \nu_{2323} = \nu_{3434} = \nu_{4343} = \kappa, \tag{4.12}$$

$$\nu_{1432} = \nu_{4123} = \nu_{3214} = \nu_{2341} = \kappa, \tag{4.13}$$

with $\kappa = g/V$.

4.1.3. Fock states

For the case of $N = 2$ fermions there are six different Fock states $|\Phi_a\rangle$

$$\begin{aligned} |\phi_1\rangle &= \hat{c}_1^\dagger \hat{c}_2^\dagger |0\rangle \qquad |\phi_2\rangle = \hat{c}_3^\dagger \hat{c}_4^\dagger |0\rangle \qquad |\phi_3\rangle = \hat{c}_1^\dagger \hat{c}_4^\dagger |0\rangle, \\ |\phi_4\rangle &= \hat{c}_2^\dagger \hat{c}_3^\dagger |0\rangle \qquad |\phi_5\rangle = \hat{c}_1^\dagger \hat{c}_3^\dagger |0\rangle \qquad |\phi_6\rangle = \hat{c}_2^\dagger \hat{c}_4^\dagger |0\rangle, \end{aligned} \tag{4.14}$$

The states $|\Phi_3\rangle$ and $|\Phi_4\rangle$ are degenerate Cooper pair states—involving two fermions with opposite momenta and opposite spins. The states $|\Phi_1\rangle$ and $|\Phi_4\rangle$ are non-magnetic, having one fermion in a spin + mode and one fermion in a spin − mode. The states $|\Phi_5\rangle$ and $|\Phi_6\rangle$ are magnetic, with both fermions in either a spin + mode or a spin − mode. These all have the same energy if fermion–fermion interactions are ignored.

4.1.4. Initial condition

We consider the case where the initial state is the pure Cooper pair state $|\Phi_3\rangle$

$$\hat{\rho}(0) = |\phi_3\rangle \langle \phi_3|, \tag{4.15}$$

with one fermion in mode $|\phi_{\mathbf{k}(+)}\rangle$ the other in mode $|\phi_{-\mathbf{k}(-)}\rangle$. The initial condition shows that the only non-zero initial stochastic averages are

$$(\overline{\tilde{g}_4 \tilde{g}_1 \tilde{g}_1^+ \tilde{g}_4^+})_{t=0} = 1 = -(\overline{\tilde{g}_4 \tilde{g}_1 \tilde{g}_4^+ \tilde{g}_1^+})_{t=0}, \tag{4.16}$$

The interaction term $\nu_{1432} \hat{c}_3^\dagger \hat{c}_2^\dagger \hat{c}_4 \hat{c}_1$ with $\nu_{1432} = g/V$ couples the Cooper pair state $|\Phi_3\rangle$ to the other Cooper pair state $|\Phi_4\rangle$, which has one fermion in the mode $|\phi_{\mathbf{k}(-)}\rangle$ and the other in mode $|\phi_{-\mathbf{k}(+)}\rangle$, so a non-zero coherence between state $|\Phi_3\rangle$ and state $|\Phi_4\rangle$ should develop. This coherence is the one to be determined and whose presence indicates coupling between Cooper pair states (each with two fermions with opposite momenta and spins) is taking place. The work of Plimak *et al* [22] shows that this leads to anomalous number correlations of the form $\langle \hat{n}_{\pm\mathbf{k}(+)} \hat{n}_{\pm\mathbf{k}(-)} \rangle - \langle \hat{n}_{\pm\mathbf{k}(+)} \rangle \langle \hat{n}_{\pm\mathbf{k}(-)} \rangle$, for the four cases $(\mathbf{K}, \mathbf{L}) = (\mathbf{k}, \mathbf{k})$, $(\mathbf{k}, -\mathbf{k})$, $(-\mathbf{k}, -\mathbf{k})$ and $(-\mathbf{k}, \mathbf{k})$. Non-zero correlations for the $(\mathbf{k}, \mathbf{k})$ and $(-\mathbf{k}, -\mathbf{k})$ cases are unexpected. The anomalous number correlations are due to the fact that true energy eigenstate is of the form $\frac{|\Phi_3\rangle \pm |\Phi_4\rangle}{\sqrt{2}}$ rather than just $|\Phi_3\rangle$ or $|\Phi_4\rangle$ [12, 24].

From the general results equations (3.49) and (3.50), the population for the Cooper pair state $|\phi_3\rangle$ and its coherence with the Cooper pair state $|\phi_4\rangle$ are given by

$$\begin{aligned} P(\Phi_3) &= \int dg^+ dg B^f(g, g^+) g_4 g_1 g_1^+ g_4^+ \\ &= \overline{\tilde{g}_4 \tilde{g}_1 \tilde{g}_1^+ \tilde{g}_4^+}, \end{aligned} \tag{4.17}$$

$$\begin{aligned} C(\Phi_4; \Phi_3) &= \int dg^+ dg B^f(g, g^+) g_4 g_1 g_2^+ g_3^+ \\ &= \overline{\tilde{g}_4 \tilde{g}_1 \tilde{g}_2^+ \tilde{g}_3^+}. \end{aligned} \tag{4.18}$$

4.1.5. The Θ^- and Θ^+ matrices

The Ito equations are given in [12] and [24] - (see equations (93), (94), and Corrigenda) and will not be repeated here. Because there is no cross-coupling between the g_i and the g_j^+ in the diffusion matrix, the overall number of Wiener increments involved is 16, which is less than the expected number $2n^2 = 32$. The Wiener increments have been numbered 1, 2, …, 16.

From inspection of the Ito equations we can then identify the elements of the Θ matrix equation (3.47) (refer also to equations (3.44) and (3.45)) that link the stochastic phase space variables between times t and $t + \delta t$. This matrix is given in two parts as follows, with Θ^- linking the $g's$ and Θ^+ linking the $g^{+'}s$.

$$\Theta^- = \begin{array}{c} \begin{matrix} \quad 1 \qquad\qquad\qquad\qquad & \quad 2 \qquad\qquad\qquad\qquad & \quad 3 \qquad\qquad\qquad\qquad & \quad 4 \qquad\qquad\qquad\qquad \end{matrix} \\ \begin{bmatrix} 1 - i\omega\delta t + \frac{\sqrt{\lambda}}{\sqrt{2}}(\delta\varpi_1 + \delta\varpi_{11}) & 0 & \frac{\sqrt{\lambda}}{\sqrt{2}}(\delta\varpi_3 + \delta\varpi_{14}) & 0 \\ 0 & 1 - i\omega\delta t + \frac{\sqrt{\lambda}}{\sqrt{2}}(\delta\varpi_6 + \delta\varpi_{16}) & 0 & \frac{\sqrt{\lambda}}{\sqrt{2}}(\delta\varpi_8 + \delta\varpi_9) \\ \frac{\sqrt{\lambda}}{\sqrt{2}}(\delta\varpi_8 + \delta\varpi_9) & 0 & 1 - i\omega\delta t + \frac{\sqrt{\lambda}}{\sqrt{2}}(\delta\varpi_1 + \delta\varpi_{11}) & 0 \\ 0 & \frac{\sqrt{\lambda}}{\sqrt{2}}(\delta\varpi_3 + \delta\varpi_{14}) & 0 & 1 - i\omega\delta t + \frac{\sqrt{\lambda}}{\sqrt{2}}(\delta\varpi_6 + \delta\varpi_{16}) \end{bmatrix} \begin{matrix} 1 \\ 2 \\ 3 \\ 4 \end{matrix} \end{array} \tag{4.19}$$

$$\Theta^{+}=$$

$$\begin{array}{c} \begin{matrix} 1 & 2 & 3 & 4 \end{matrix} \\ \begin{bmatrix} 1+i\omega\delta t+\frac{\sqrt{\lambda^*}}{\sqrt{2}}(\delta\widetilde{\omega}_1^{+}+\delta\widetilde{\omega}_{11}^{+}) & 0 & \frac{\sqrt{\lambda^*}}{\sqrt{2}}(\delta\widetilde{\omega}_3^{+}+\delta\widetilde{\omega}_{14}^{+}) & 0 \\ 0 & 1+i\omega\delta t+\frac{\sqrt{\lambda^*}}{\sqrt{2}}(\delta\widetilde{\omega}_6^{+}+\delta\widetilde{\omega}_{16}^{+}) & 0 & \frac{\sqrt{\lambda^*}}{\sqrt{2}}(\delta\widetilde{\omega}_8^{+}+\delta\widetilde{\omega}_9^{+}) \\ \frac{\sqrt{\lambda^*}}{\sqrt{2}}(\delta\widetilde{\omega}_8^{+}+\delta\widetilde{\omega}_9^{+}) & 0 & 1+i\omega\delta t+\frac{\sqrt{\lambda^*}}{\sqrt{2}}(\delta\widetilde{\omega}_1^{+}+\delta\widetilde{\omega}_{11}^{+}) & 0 \\ 0 & \frac{\sqrt{\lambda^*}}{\sqrt{2}}(\delta\widetilde{\omega}_3^{+}+\delta\widetilde{\omega}_{14}^{+}) & 0 & 1+i\omega\delta t+\frac{\sqrt{\lambda^*}}{\sqrt{2}}(\delta\widetilde{\omega}_6^{+}+\delta\widetilde{\omega}_{16}^{+}) \end{bmatrix} \begin{matrix} 1 \\ 2 \\ 3 \\ 4 \end{matrix} \end{array} \tag{4.20}$$

These matrices only involve c-numbers. Here $\lambda = \frac{\kappa}{i\hbar}$.

Applying the theory presented in previous sections for the Ito stochastic equations gives the coherence between the two Cooper pair states at time $t = \delta t$ as

$$\begin{aligned} C(\Phi_4;\,\Phi_3)_{t=\delta t} = \Bigg[& \left\{\left(1-i\omega\delta t)+\frac{\sqrt{\lambda}}{\sqrt{2}}(\delta\widetilde{\omega}_6+\delta\widetilde{\omega}_{16}\right)\right\}\times\left\{\left(1-i\omega\delta t)+\frac{\sqrt{\lambda}}{\sqrt{2}}(\delta\widetilde{\omega}_1+\delta\widetilde{\omega}_{11}\right)\right\} \\ & \times\left\{\frac{\sqrt{\lambda^*}}{\sqrt{2}}(\delta\widetilde{\omega}_8^{+}+\delta\widetilde{\omega}_9^{+})\right\}\times\left\{\frac{\sqrt{\lambda^*}}{\sqrt{2}}(\delta\widetilde{\omega}_8^{+}+\delta\widetilde{\omega}_9^{+})\right\}\Bigg]_{Stochastic\ Avg} \\ & \times(\overline{\widetilde{g}_4\widetilde{g}_1\widetilde{g}_4^{+}\widetilde{g}_1^{+}})_{t\,=\,0}. \end{aligned} \tag{4.21}$$

A direct evaluation of the stochastic average provides an expression for the short time behaviour of the coherence. There are terms involving the stochastic averages of products of two, three and four Wiener increments. Those involving three are always zero. Those involving four are sums of products of stochastic averages of two Wiener increments. These are zero because those products involving $\delta\widetilde{\omega}_6, \ldots, \delta\widetilde{\omega}_{11}$ such as $\overline{\delta\widetilde{\omega}_6\delta\widetilde{\omega}_{11}} = \overline{\delta\widetilde{\omega}_{11}\delta\widetilde{\omega}_6} = \ldots = \overline{\delta\widetilde{\omega}_{11}\delta\widetilde{\omega}_9}$ are all zero. From equations (3.37)–(3.39), $\overline{\delta\widetilde{\omega}_8^{+}\delta\widetilde{\omega}_9^{+}} = \overline{\delta\widetilde{\omega}_9^{+}\delta\widetilde{\omega}_8^{+}} = 0$ and the only non-zero contributions are $\overline{\delta\widetilde{\omega}_8^{+}\delta\widetilde{\omega}_8^{+}} = \overline{\delta\widetilde{\omega}_9^{+}\delta\widetilde{\omega}_9^{+}} = \delta t$. Using equation (4.16) we can obtain the coherence between two Cooper pair states $|\phi_3\rangle$ and state $|\phi_4\rangle$ correct to order δt as

$$C(\Phi_4;\,\Phi_3)_{t=\delta t} = (g/i\hbar V)\delta t. \tag{4.22}$$

This result demonstrates the onset of coherence between two Cooper pair states, one with a fermion in each of $\phi_{\mathbf{k},+}$, $\phi_{-\mathbf{k},-}$ and other with a fermion in each of $\phi_{\mathbf{k},-}$, $\phi_{-\mathbf{k},+}$. Note that the result is independent of the free-evolution frequency ω.

4.2. Analytical results

4.2.1. Elimination of free time evolution and dimmensionless time variables

From the form of the coupling matrices we see that the free evolution for all four modes has the same frequency ω, and as we have just seen ω does not appear in the result for the short time coherence. To simplify the numerical calculation of the coherence, one can eliminate the free evolution frequency ω from the Ito stochastic equations in [24] (see equations (93), (94), and Corrigenda).

Writing

$$\widetilde{h}_i(t) = \widetilde{g}_i(t)e^{i\omega t}, \qquad \widetilde{h}_i^{+}(t) = \widetilde{g}_i^{+}(t)e^{-i\omega t}, \tag{4.23}$$

we first note that

$$\overline{\widetilde{g}_i\widetilde{g}_k\widetilde{g}_l^{+}\widetilde{g}_m^{+}} = \overline{\widetilde{h}_i\widetilde{h}_k\widetilde{h}_l^{+}\widetilde{h}_m^{+}}\ \ldots etc, \tag{4.24}$$

for equal numbers of $\widetilde{h}$ and $\widetilde{h}^{+}$.

We also introduce the dimensionless time variables δT given by $(g/\hbar V)\delta t$, and $T = (g/\hbar V)t$. The Wiener increments $\delta\widetilde{\omega}_a$ are replaced by $\delta\widetilde{\Omega}_a$, now normalized in dimensionless interval δT.

4.2.2. Ito equations for new stochastic variables

We can then show that by substituting equation (4.23) into the Ito equations (see equations (93) and (94) and Corrigenda in [24])

$$\tilde{h}_1(T+\delta T) = \Theta^-_{1,1}\tilde{h}_1(T) + \Theta^-_{1,3}\tilde{h}_3(T), \qquad \tilde{h}_1^+(T+\delta T) = \Theta^+_{1,1}\tilde{h}_1^+(T) + \Theta^+_{1,3}\tilde{h}_3^+(T),$$
$$\tilde{h}_2(T+\delta T) = \Theta^-_{2,2}\tilde{h}_2(T) + \Theta^-_{2,4}\tilde{h}_4(T), \qquad \tilde{h}_2^+(T+\delta T) = \Theta^+_{2,2}\tilde{h}_1^+(T) + \Theta^+_{2,4}\tilde{h}_4^+(T),$$
$$\tilde{h}_3(T+\delta T) = \Theta^-_{3,1}\tilde{h}_1(T) + \Theta^-_{3,3}\tilde{h}_3(T), \qquad \tilde{h}_3^+(T+\delta T) = \Theta^+_{3,1}\tilde{h}_1^+(T) + \Theta^+_{3,3}\tilde{h}_3^+(T),$$
$$\tilde{h}_4(T+\delta T) = \Theta^-_{4,2}\tilde{h}_2(T) + \Theta^-_{4,4}\tilde{h}_4(T), \qquad \tilde{h}_4^+(T+\delta T) = \Theta^+_{4,2}\tilde{h}_2^+(T) + \Theta^+_{4,4}\tilde{h}_4^+(T). \tag{4.25}$$

where, with the new Wiener increments defined by $\delta\widetilde{\Omega} = \sqrt{g/\hbar V}\times\delta\widetilde{\omega}$, the non zero $\Theta^-_{\alpha,\beta}$ are

$$\Theta^-_{1,1} = 1 + \frac{1}{\sqrt{2i}}(\delta\widetilde{\Omega}_1 + \delta\widetilde{\Omega}_{11}), \qquad \Theta^-_{1,3} = \frac{1}{\sqrt{2i}}(\delta\widetilde{\Omega}_3 + \delta\widetilde{\Omega}_{14}),$$
$$\Theta^-_{2,2} = 1 + \frac{1}{\sqrt{2i}}(\delta\widetilde{\Omega}_6 + \delta\widetilde{\Omega}_{16}), \qquad \Theta^-_{2,4} = \frac{1}{\sqrt{2i}}(\delta\widetilde{\Omega}_8 + \delta\widetilde{\Omega}_9),$$
$$\Theta^-_{3,1} = \frac{1}{\sqrt{2i}}(\delta\widetilde{\Omega}_8 + \delta\widetilde{\Omega}_9), \qquad \Theta^-_{3,3} = 1 + \frac{1}{\sqrt{2i}}(\delta\widetilde{\Omega}_1 + \delta\widetilde{\Omega}_{11}),$$
$$\Theta^-_{4,2} = \frac{1}{\sqrt{2i}}(\delta\widetilde{\Omega}_3 + \delta\widetilde{\Omega}_{14}), \qquad \Theta^-_{4,4} = 1 + \frac{1}{\sqrt{2i}}(\delta\widetilde{\Omega}_6 + \delta\widetilde{\Omega}_{16}), \tag{4.26}$$

and $\Theta^+_{i,j} = (\Theta^-_{i,j})^*$ and $\delta\widetilde{\Omega}_i \to \delta\widetilde{\Omega}_i^+$. This eliminates ω from the calculation.

4.2.3. Two body QCF –special QCF for Cooper pair states populations and coherences
The $C(\Phi_4;\,\Phi_3)$ coherence is then given by

$$C(\Phi_4;\,\Phi_3) = \overline{\tilde{h}_4\tilde{h}_1\tilde{h}_2^+\tilde{h}_3^+}. \tag{4.27}$$

In terms of the new quantities the coherence for a small time interval with $\delta T \ll 1$ is now based on the general expression

$$C(\Phi_4;\,\Phi_3)_{T=\delta T} = \Bigg[\left\{1 + \frac{1}{\sqrt{2i}}(\delta\widetilde{\Omega}_6 + \delta\widetilde{\Omega}_{16})\right\}\times\left\{1 + \frac{1}{\sqrt{2i}}(\delta\widetilde{\Omega}_1 + \delta\widetilde{\Omega}_{11})\right\}$$
$$\times\left\{\frac{1}{(\sqrt{2i})^*}(\delta\widetilde{\Omega}_8^+ + \delta\widetilde{\Omega}_9^+)\right\}\times\left\{\frac{1}{(\sqrt{2i})^*}(\delta\widetilde{\Omega}_8^+ + \delta\widetilde{\Omega}_9^+)\right\}\Bigg]_{Stochastic\ Avg}$$
$$\times\,(\overline{\tilde{h}_4\tilde{h}_1\tilde{h}_4^+\tilde{h}_1^+})_{T=0}, \tag{4.28}$$

where $(\overline{\tilde{h}_4\tilde{h}_1\tilde{h}_4^+\tilde{h}_1^+})_{T=0} = 1$.

Applying the same stochastic averaging techniques as in section 4.1.5, we confirm that the short time coherence between two Cooper pair state $|\phi_3\rangle$ and state $|\phi_4\rangle$ correct to order δt is

$$C(\Phi_4;\,\Phi_3)_{t=\delta t} = \frac{1}{i}\delta T = (g/i\hbar V)\delta t. \tag{4.29}$$

As a first test of numerical calculations using Grassmann phase space theory we will evaluate the coherence numerically for a small time interval with $\delta T \ll 1$ based on the expression in equation (4.28).

4.2.4. Analytic results for the M matrix in terms of dimensionless time increment
For the Fock states $|\phi_3\rangle$ and state $|\phi_4\rangle$ the populations are specified by X_{15}, X_{22} and coherences by X_{16}, X_{21}.

$$X_{15} = \overline{\tilde{h}_4\tilde{h}_1\tilde{h}_1^+\tilde{h}_4^+} = P(\Phi_3); \quad X_{16} = \overline{\tilde{h}_4\tilde{h}_1\tilde{h}_2^+\tilde{h}_3^+} = C(\Phi_4;\,\Phi_3); \quad X_{21} = \overline{\tilde{h}_3\tilde{h}_2\tilde{h}_1^+\tilde{h}_4^+} = C(\Phi_3;\,\Phi_4);$$
$$X_{22} = \overline{\tilde{h}_3\tilde{h}_2\tilde{h}_2^+\tilde{h}_3^+} = P(\Phi_4).$$

Coherences and populations invoving the other four Fock states $|\phi_1\rangle$, $|\phi_2\rangle$, $|\phi_5\rangle$ and $|\phi_6\rangle$ are specified by other X_k 's. A list of all the components of the X vector is given in appendix B.

Our focus is on determining the coherence between $|\phi_3\rangle$ and $|\phi_4\rangle$, given by X_{16}. As only the population of $|\phi_3\rangle$, given byX_{15} is initially non-zero, then the short-time coupling to the coherence X_{16} will be determined by the matrix element $M(16,15)$. Hence we first determine this matrix element, using the same approach as in section 4.1.4.

$$
\begin{aligned}
M(16,\,15) &= (-1)\overline{\Theta^{-}_{4,4}\Theta^{-}_{1,1}\Theta^{+}_{2,4}\Theta^{+}_{3,1}}. \\
&= (-1)\Bigg[\left(1+\frac{1}{\sqrt{2i}}(\delta\widetilde{\Omega}_{6}+\delta\widetilde{\Omega}_{16})\right)\left(1+\frac{1}{\sqrt{2i}}(\delta\widetilde{\Omega}_{1}+\delta\widetilde{\Omega}_{11})\right) \\
&\quad\times\left(\frac{1}{(\sqrt{2i})^{*}}(\delta\widetilde{\Omega}^{+}_{8}+\delta\widetilde{\Omega}^{+}_{9})\right)\left(\frac{1}{(\sqrt{2i})^{*}}(\delta\widetilde{\Omega}^{+}_{8}+\delta\widetilde{\Omega}^{+}_{9})\right)\Bigg]_{StochAvg} \\
&= (-1)\left(\frac{1}{(\sqrt{2i})^{*}}\right)^{2}\overline{(\delta\widetilde{\Omega}^{+}_{8}+\delta\widetilde{\Omega}^{+}_{9})(\delta\widetilde{\Omega}^{+}_{8}+\delta\widetilde{\Omega}^{+}_{9})} \\
&= (-1)\frac{1}{(2i)^{*}}(\overline{(\delta\widetilde{\Omega}^{+}_{8})^{2}}+\overline{(\delta\widetilde{\Omega}^{+}_{9})^{2}}) \\
&= (-1)\frac{1}{-2i}(\delta T+\delta T) \\
&= \frac{1}{i}(\delta T).
\end{aligned}
\tag{4.30}
$$

This shows that the population X_{15} is coupled to the coherence X_{16} to order δT. Using a similar approach we can evaluate all the elements in the column 15 for the M matrix. This shows that the only non-zero elements in this column are M(15, 15), M(16,15), M(21, 15) - M(22,15) is zero, so the population X_{15} is also coupled to the other coherence X_{21} and to itself to order δT. We can then similarly evaluate all the elements in the column 16 to find that the only non-zero elements are M(15, 16), M(16, 16), M(22, 16) - M(21,16) is zero, so the coherence X_{16} is also coupled to the populations X_{22} and X_{15} and to itself to order δT. Continuing in this way we find that for columns 15, 16, 21 and 22 of the M matrix the only non-zero elements are M(15, 15), M(16, 15), M(21, 15) and M(22,15)(=0) ; M(15, 16), M(16, 16), M(21,16)(=0) and M(22, 16); M(15, 21), M(16,21)(=0), M(21, 21) and M(22,21); and M(15,22)(=0), M(16, 22), M(21, 22) and M(22,2). Some elements are of order δT^{2}, and these are zero to order δT. Results for the evaluation of the elements in column 15 - M(15, 15), M(21, 15), M(22,15), M(36,15) are typical, and can be found in appendix C. This means that coherences and populations other than those specified by X_{15}, X_{22} and X_{16}, X_{21} will not be coupled to the initial population X_{15} , so only the 4 × 4 sub-matrix of M specified by these elements will be required to determine the evolution of the populations X_{15}, X_{22} and coherences X_{16}, X_{21}. This saved wasting time determining numerically all 36 × 36 elements of M.

To show this more formally to be the case for finite time $T = n \cdot \delta T$ we have (in an obvious notation)

$$X_{u}(T) = M(u,\,v)M(v,\,w).....M(y,\,z)M(z,\,15)X_{15}(0) \tag{4.31}$$

where the column or row indices v, w, …, y, z are summed over. If the elements in the column 15 for M are zero except for those in rows $z = 15, 16, 21, 22$ then in the first step M(z,15) $X_{15}(0)$ will only be non-zero for $z = 15, 16, 21, 22$. If in addition the elements in columns 16, 21, 22 are also zero except for those in rows $y = 15, 16, 21, 22$ then after the second step M(y,z) M(z,15) $X_{15}(0)$ will only be non-zero for $y = 15, 16, 21, 22$. So with all elements in the columns 15, 16, 21, 22 zero except for those in rows 15, 16, 21, 22, we see that subsequent steps leading to $X_{u}(T)$ can only give a non-zero result for $u = 15, 16, 21, 22$. This shows that if all elements of the 15, 16, 21, 22 columns of M are zero outside of those in the 4 × 4 submatrix with these columns and with rows 15, 16, 21, 22, then the evolution from the initial state $|\phi_{3}\rangle$ (corresponding to $X_{15}(0) = 1$) could only give non-zero results for the populations and coherences of $|\phi_{3}\rangle$ and state $|\phi_{4}\rangle$. Hence this confirms that only the elements within the 4 × 4 submatrix of M with rows and columns 15, 16, 21, 22 are relevant to the evolution of these populations and coherences.

4.2.5. Symmetry of matrix M

When evaluated analytically the matrix M can be shown to be symmetric. If the matrix element $M_{\alpha,\beta}$ is given by

$$M_{a,\beta} = \Theta^{-}_{i,j}\cdot\Theta^{-}_{k,l}\cdot\Theta^{+}_{m,n}\cdot\Theta^{+}_{p,q}\cdot(-1)^{P}, \tag{4.32}$$

then $M_{\beta,\alpha}$ is obtained via

$$M_{\beta,\alpha} = \Theta^{-}_{j,i}\cdot\Theta^{-}_{l,k}\cdot\Theta^{+}_{n,m}\cdot\Theta^{+}_{q,p}\cdot(-1)^{P}. \tag{4.33}$$

Also, if $M_{\alpha,\beta} = 0$ then $M_{\beta,\alpha} = 0$. Although the $\Theta^{\pm}_{a,b}$ may involve different Wiener increments $(\delta\widetilde{\Omega})^{\pm}_{r}$ to those in the $\Theta^{\pm}_{b,a}$ they can be seen to be in one-one correspondence, so when stochastic averaging occurs the outcome is the same. This leads to the symmetry result

$$M_{a,\beta} = M_{\beta,a}. \tag{4.34}$$

A comparison of the expressions for $M_{15,\,16}$ and $M_{16,15}$ illustrates the situation.

4.2.6. Expression for 4 × 4 submatrix of M

Using the analytic results for the 16 elements of the 4 × 4 submatrix in terms of dimensionless time increments given in section 3.2.6 and apppendix C, we obtain its analytic form for Cooper pair states populations and coherences. With

$$\begin{pmatrix} X_{15} \\ X_{16} \\ X_{21} \\ X_{22} \end{pmatrix}_{\delta T} = \begin{pmatrix} M_{15,15} & M_{15,16} & M_{15,21} & M_{15,22} \\ M_{16,15} & M_{16,16} & M_{16,21} & M_{16,22} \\ M_{21,15} & M_{21,16} & M_{21,21} & M_{21,22} \\ M_{22,15} & M_{22,16} & M_{22,21} & M_{22,22} \end{pmatrix} \begin{pmatrix} X_{15} \\ X_{16} \\ X_{21} \\ X_{22} \end{pmatrix}_0, \tag{4.35}$$

and $\lambda = g/i\hbar V$, the analytic form of M is given by

$$M = \begin{pmatrix} 1 & 1/i\delta T & -1/i\delta T & 0 \\ 1/i\delta T & 1 & 0 & -1/i\delta T \\ -1/i\delta T & 0 & 1 & 1/i\delta T \\ 0 & -1/i\delta T & 1/i\delta T & 1 \end{pmatrix}, \tag{4.36}$$

after dimensionless units defined by $\delta T = \frac{g}{\hbar V}\delta t$ have been introduced. Note that the analytic form of M is indeed symmetric.

4.2.7. Analytic results for eigenvalues, eigenvectors for the 4 × 4 M submatrix

For the analytic form of M given in equation (4.36), the eigenvalues and the eigenvectors are

$$\mu_1 = 1 + i2\delta T, \quad \mu_2 = 1 + i.0\delta T, \quad \mu_3 = 1 + i.0\delta T, \quad \mu_4 = 1 - i2\delta T \tag{4.37}$$

corresponding respectively to the normalized eigenvectors

$$\xi_1 = \frac{1}{\sqrt{4}}\begin{pmatrix} -1 \\ +1 \\ -1 \\ +1 \end{pmatrix} \quad \xi_2 = \frac{1}{\sqrt{2}}\begin{pmatrix} 1 \\ 0 \\ 0 \\ 1 \end{pmatrix} \quad \xi_3 = \frac{1}{\sqrt{2}}\begin{pmatrix} 0 \\ 1 \\ 1 \\ 0 \end{pmatrix} \quad \xi_4 = \frac{1}{\sqrt{4}}\begin{pmatrix} -1 \\ -1 \\ +1 \\ +1 \end{pmatrix}. \tag{4.38}$$

Hence the quantities defined in equation (3.63) are $r_1 = r_2 = r_3 = r_4 = 1$ and $a_1 = 2$, $a_2 = 0$, $a_3 = 0$, $a_4 = -2$.

4.2.8. Finite time evolution for the $C(\Phi_4; \Phi_3)$ coherence

Using equation (3.65) above one finds for $(M)^n_{16,15}$

$$\begin{aligned} (M)^n_{16,15} &= \sum_\mu e^{ia_\mu T} Y_{\mu,16} Y_{\mu,15} (r_\mu)^{T/\delta T} \\ &= e^{i(+2)T}\frac{(+1)}{\sqrt{4}}\frac{(-1)}{\sqrt{4}} + e^{i(-2)T}\frac{(-1)}{\sqrt{4}}\frac{(-1)}{\sqrt{4}} \\ &\quad + e^{i(0)T}\frac{(0)}{\sqrt{2}}\frac{(+1)}{\sqrt{2}} + e^{i(0)T}\frac{(1)}{\sqrt{2}}\frac{(0)}{\sqrt{2}}. \end{aligned} \tag{4.39}$$

Therefore

$$\begin{aligned} (M)^n_{16,15} &= -\frac{1}{4}e^{-i2T} + \frac{1}{4}e^{+i2T} \\ &= \frac{1}{2i}\sin 2T. \end{aligned} \tag{4.40}$$

Hence

$$\begin{aligned} C(\phi_4; \phi_3) &= (M)^n_{16,15}(X_{15})_0 \\ &= \frac{1}{2i}\sin 2T, \end{aligned} \tag{4.41}$$

since $(X_{15})_0 = 1$. The result in equation (4.41) is in dimensionless units. Thus the analytic form of the finite time coherence has a sinusoidal time dependence. We see that the coherence does not depend on the free evolution frequency ω, confirming the correctness of the above elimination of the free time evolution. The short time coherence in equation (4.29) is easily confirmed by replacing T by δT. The finite time coherence result in equation (4.41) can also be obtained via a standard matrix mechanics treatment based on the Hamiltonian in equation (4.9).

4.3. Numerical results

As indicated above, we have introduced a dimensionless time variable δT given by $(g/hV)\,\delta t$, and the coherence will now be calculated numerically in the case of the short time regime for various δT. The new Wiener increments $\delta\widetilde{\Omega}_a$ are normalized as in equation (3.36), but now with the interval being the dimensionless quantity δT. The stochastic

average in equation (3.52) or (4.28) that is involved in calculating the coherence as a function of dimensionless time δT will now be carried out numerically based on the fundamental definition (equation (3.25)) of a stochastic average. The result for short time δT should be proportional to δT (with a factor $1/i$). The calculations were carried out using MatLab, which allowed us to run six labs in parallel. The stochastic averaging was carried out over $m = 1000$ trajectories in each lab, and in each trajectory the normalized Wiener increments are obtained using the MatLab command mvnrnd. for which the mean values of the random variables is set as zero and the covariance is set to $\sqrt{\delta T}$. Two other MatLab commands can be used for the same purpose, namely normrnd and randn for which the mean values of the random values is set to zero and the standard deviation is set to $\sqrt{\delta T}$. We display a plot of the numerically calculated coherence between states ϕ_3 and ϕ_4 for various choices of δT in units of $1/i$ and for cases of $m = 1000$ trajectories in each case. The analytic result from equation (4.29) is also shown. The results have shown that the numerical calculation of the coherence agrees well with the analytic formula.

We then calculate the same coherence, but now for a finite time interval with T ranging from 0 to π and based on using equations (3.65), and with the same initial condition. We will compare the result with the analytic expression given by equation (4.41). All calculations were carried out using a standard desk-top computer with parallel processing facilities.

4.3.1. Numerical stochastic calculations of elements in 4 × 4 M submatrix–$\delta T = 0.01$

In this section the M matrix is now calculated stochastically based on the formula (3.54) set out in section 3.3.2. The programming issues are discussed below in appendix D. Here we will only present results. Table 1 shows typical results for the elements $M(15, 15)$, $M(15, 16)$, $M(15, 21)$ and $M(15, 22)$ in the row 15 of the important 4×4 submatrix of matrix M when the time increment is $\delta T = 0.01$, and for the parallel processing run over six labs where the ensemble size was $m = 1000$ in each lab. The table shows the percentage error (std error, average error) is given by the magnitude of the difference between the stochastically determined value and the analytic value, expressed as a percentage of the analytic value. The standard deviation is defined in the usual way based on the difference in the results for each of the six labs from the analytic result, again expressed as a percentage of the analytic result. The overall averages for each element are also given as well as an estimate of their percentage errors. The tables for rows 16, 21 and 22 of the 4×4 submatrix of M are set out in appendix C.

Table 1. Table shows the numerical results for the imag and real parts of $M(15, 15)$,$M(15, 16)$, $M(15, 21)$, $M(15,22)$ across the 6 parallel processing labs. The results were obtained using the MatLab parallel processing program for M 4×4 matrix. The average matrix element, the average error and the σ error are also shown for each of these matrix elements. The remaining elements of Rows 16, 21, 22 are given in appendix C, tables C1–C3

M(Alpha,Beta) Row 15

PP _Run_1 m = 1000	δT = 0.01							
	M(15, 15) $(44\_11\_11\_44)_{Stoch}$		M(15, 16) $(-44\_11\_13\_42)_{Stoch}$		M(15, 21) $(-42\_13\_11\_44)_{Stoch}$		M(15, 22) $(42\_13\_13\_42)_{Stoch}$	
	Real	Img	Real	Img	Real	Img	Real	Img
Lab1	0.994628272	−0.001412707	−0.000035235	−0.010266260	0.000139789	+0.010152874	0.000109803	+0.000000000
Lab2	1.003941551	+0.000283385	0.000015882	−0.009033418	−0.000091416	+0.010813706	0.000093806	+0.000000000
Lab3	0.998606186	−0.002130266	−0.000005336	−0.010379494	0.000100779	+0.010239848	0.000100651	+0.000000000
Lab4	1.004606801	+0.001032299	−0.000062297	−0.010062040	−0.000047954	+0.010520640	0.000106743	+0.000000000
Lab5	1.002122085	−0.000282594	0.000030534	−0.009314542	0.000094503	+0.009805886	0.000084811	+0.000000000
Lab6	0.999249308	−0.001128745	−0.000020466	−0.010934714	−0.000083637	+0.010706543	0.000116638	+0.000000000
Avg. Value	1.0005257 −0.000606438i		−0.00001281966 −0.009998411i		0.00001867733 + 0.010373249i		1.020753e−04	
Avg Error %	0.3031			5.4909		4.3795	9.2030	
σ Error %	0.3479			6.4506		5.0842	10.7074	

4.3.2. The numerical stochastic result for the M 4 × 4 submatrix

The numerical calculation for the matrix M 4×4 submatrix for $\delta T = 0.01$ gave the following result.

$$M= \begin{matrix} \\ 15 \\ 16 \\ 21 \\ 22 \end{matrix} \begin{matrix} \begin{matrix} 15 & \quad 16 & \quad 21 & \quad 22 \end{matrix} \\ \begin{pmatrix} 1.00053 - 0.000606438i & -0.0000128197 - 0.00999841i & 0.0000186773 + 0.0103732i & 0.000102075 + 0.i \\ -0.000011952 - 0.010018i & 1.00053 - 0.000606438i & 0.000107978 + 0.i & 0.0000186773 + 0.0103732i \\ 0.0000281993 + 0.0096536i & 0.000096366 + 0.i & 1.00053 - 0.000606438i & -0.0000128197 - 0.00999841i \\ 0.000103714 + 0.i & 0.0000281993 + 0.0096536i & -0.000011952 - 0.010018i & 1.00053 - 0.000606438i \end{pmatrix} \end{matrix} \begin{matrix} \\ 15 \\ 16 \\ 21 \\ 22 \end{matrix} \tag{4.42}$$

Equation (4.42) shows the M matrix containing the numerical results for the imag and real parts of $M(15, 15)$,$M(15, 16)$, $M(15, 21)$, $M(15, 22)$ across the 6 parallel processing labs for $\delta T = 0.01$.

Inspection of the above 4×4 submatrix of M in equation (4.42) reveals certain symmetries in the numerical results. Namely, the matrix element $M(15, 15)$ is equal in value to that of $M(16, 16)$ and so is the case for $M(21, 21)$ and $M(22, 22)$, $M(15, 16)$ and $M(21, 22)$ and ($M21, 15$) and $M(22, 16)$. The explanation of this is given in appendix C.3.

4.3.3. Numerical results for eigenvalues, eigenvectors for the 4×4 *M submatrix*

For reasons described in section 4.2.4 only the elements of the 4×4 submatrix of M for rows 15, 16, 21 and 22 needed to be determined numerically, resulting in the matrix shown in equation (4.42). The eigenvalues, eigenvectors of this matrix and its transpose will now be determined.

The tables 2–4 present the numerical results for the normalized eigenvectors for the stochastically determined M and M^T along with the eigenvalues and other quantities. In addition the results of calculating the M matrix using equation (3.60) is also shown. The result for the M matrix may be compared with that in the analytical form of M given by equation (4.36).

Numerical results for the eigenvalues of the 4×4 M (or M^T) matrix

Table 2. Table shows the eigenvalues for the numerically calculated M or (M^T) from the matrix as in tables 1 and C1–C3, (see also equation (4.42)). The results were obtained using the MatLab parallel processing M 4×4 matrix program for $\delta T = 0.01$ and $m = 1000$. A separate Mathematica notebook was used for the biorthogonality calculation.

	Matrix M or M^T		
U = 1	U = 2	U = 3	U = 4
1.000 459 204 7 + 0.019 408 740 2*i*	1.000 639 455 6 − 0.000 607 701 2*i*	1.000 616 958 6 − 0.000 605 173 6*i*	1.000 387 182 9 − 0.020 621 617 2*i*

Numerical results for the normalized eigenvectors of the 4×4 M submatrix

Table 3. Table shows the normalized eigenvectors for the numerically calculated M 4×4 matrix as in tables 1 and C1–C3 . The results were obtained using the MatLab parallel processing M 4×4 matrix program for $\delta T = 0.01$ and $m = 1000$. A separate Mathematica notebook was used for the biorthogonality calculation.

	Matrix M Normalised Eigenvectors		
ξ_1	ξ_2	ξ_3	ξ_4
− 0.508 654 768 3 − 0.000 020 846 2*i*	0.519 242 300 4 + 0.001 293 334 9*i*	− 0.497 842 037 4 + 0.001 091 514 6*i*	0.508 651 874 0 + 0.000 231 187 0*i*
0.509 155 519 3 + 0.000 195 526 0*i*	0.498 329 763 6 − 0.001 010 689*i*	0.519 755 336 32 + 0.001 260 703 4*i*	0.509 152 537 3 − 0.000 102 135 4*i*
− 0.490 691 741 0 + 0.000 208 146 2*i*	0.480 264 246 1 − 0.001 485 615 6*i*	0.500 908 580 4 + 0.001 124 057 0*i*	− 0.490 694 810 7 + 0.000 098 521 8*i*
0.491 174 797 0 − 0.000 016 330 4*i*	0.501 405 244 5 + 0.001 088 122 7*i*	0.480 733 091 5 + 0.001 403 908 5*i*	− 0.491 177 872 0 + 0.000 246 859 8*i*

Numerical results for the normalized eigenvectors of the 4×4 M^T submatrix

Table 4. Table shows the normalized eigenvectors for the numerically calculated M^Tas in tables 1 and C1–C3 . The results were obtained using the MatLab parallel processing M 4×4 matrix program for $\delta T = 0.01$ and $m = 1000$. A separate Mathematica notebook was used for the biorthogonality calculation.

	Matrix M^T Normalised Eigenvectors		
η_1	η_2	η_3	η_4
− 0.491 492 446 8 + 0.000 008 370 5*i*	0.501 728 459 0 + 0.001 101 114 5*i*	− 0.481 044 734 4 + 0.001 397 193 8*i*	0.491 495 265 5 − 0.000 235 159 7*i*
0.491 009 081 6 − 0.000 200 318 2*i*	0.480 573 894 8 − 0.001 474 801 1*i*	0.501 233 261 4 + 0.001 132 730 4*i*	0.491 011 888 4 − 0.000 086 737 4*i*
−0.509 484 794 0 − 0.000 203 914 7*i*	0.498 651 046 9 − 0.000 999 125 8*i*	0.520 092 231 9 + 0.001 269 764 3*i*	− 0.509 481 537 1 − 0.000 114 495 0*i*
0.508 983 722 1 + 0.000 029 113 8*i*	0.519 577 008 9 + 0.001 306 896 3*i*	− 0.498 164 765 8 + 0.001 084 326 0*i*	− 0.508 980 547 2 − 0.000 243 618 0*i*

Numerical results for quantities r, a

Table 5. Table shows the values of a_u and r_u (refer to equations (3.63), (3.65)) for the M 4×4 matrix. The results were obtained using the MatLab parallel processing M 4×4 matrix program for $\delta T = 0.01$ and $m = 1000$. A separate Mathematica notebook was used for the biorthogonality calculation.

a_u and r_u values			
a_1	a_2	a_3	a_4
1.939 739 854 8	−0.060 731 285 6	−0.060 480 046 1	−2.061 071 704 0
r_1	r_2	r_3	r_4
1.000 647 450 2	1.000 639 640 1	1.000 617 141 6	1.000 599 703 5

The results in table 5 are used in the calculations of the finite time behaviour of the coherence $C(\phi_4; \phi_3)$.

4.3.4. Numerical re-determination of 4×4 M *matrix*

In this subsection we confirm that the eigenvectors and eigenvalues for M and M^T are accurate enough to reconstruct via (3.60) the original matrix M from which they were obtained. This is an important check for the accuracy of the numerical determination of the finite time behaviour.

After the nomalization of the eigenvectors of the matrices M and M^T, the re-determined matrix M is given by

Table 6. Table shows the elements of the numerically calculated M using equation (3.60) and the eigenvectors shown in tables 3 and 4. The eigenvalues used are as in table 2. The results were obtained using the parallel processing MatLab M 4×4 matrix program for $\delta T = 0.01$ and $m = 1000$.

	Numerical M Matrix			
	C 15	C 16	C 21	C22
R 15	$1.000\,526 - 0.000\,06i$	$-0.000\,013 - 0.009\,998i$	$0.000\,019 + 0.010\,373i$	$0.000\,102 + 0.i$
R 16	$-0.000\,012 - 0.010\,018i$	$1.000\,526 - 0.000\,606i$	$0.000\,108 + 0.i$	$0.000\,019 + 0.010\,373i$
R 21	$0.000\,028 + 0.009\,654i$	$0.000\,096 + 0.i$	$1.000\,526 - 0.000\,606i$	$-0.000\,013 - 0.009\,998i$
R 22	$0.000\,104 + 0.i$	$0.000\,028\,2 + 0.009\,654i$	$-0.000\,012 - 0.010\,018i$	$1.000\,526 - 0.000\,606i$

The results in table 6 for the matrix elements of the 4×4 submatrix of M may be compared with equation (4.42) and confirm that the expression in equation (3.60) in terms of the normalized eigenvectors and eigenvalues results in an M with matrix elements which are consistent with the numerical stocahastic matrix elements listed in equation (4.42).

4.3.5. Numerical results for short time coherence $C(\phi_4; \phi_3)$ *–effects of* m, δT

In this subsection we consider the effect on the accuracy of the numerical results for the short time coherence of varying the ensemble size for the stochastic calculations and of changing the time interval. It was expected that the accuracy would improve as the ensemble size becomes larger, and that for a given ensemble size the accuracy

Table 7. Table shows the std error for the numerically calculated *imag*(C) across the 6 parallel processing labs, for $\delta T \ll 1$. The results were obtained in run1 for the MatLab parallel processing $C(\phi_4; \phi_3)$ program for $\delta T \in [0,\ 0.01]$ and $m = 100{,}300{,}{,}1000$.

The percentage error tables for $C(\Phi_4;\Phi_3)$, M = 10, 100, 300, 1000 for δT = 0.01 R1

PP _Run_1	$\delta T = 0.01$							
	M = 10		M = 100		M = 300		M = 1000	
	Img(C)	Std_Error	Img(C)	Std_Error	Img(C)	Std_Error	Img(C)	Std_Error
Lab1	−0.017508994	75.0899%	−0.011305942	13.0594%	−0.009977968	0.2203%	−0.009881590	1.1841%
Lab2	−0.008375224	16.2478%	−0.009473180	5.2682%	−0.010710466	7.1047%	−0.010367382	3.6738%
Lab3	−0.007840392	21.5961%	−0.008266465	17.3354%	−0.009146746	8.5325%	−0.009901375	0.9862%
Lab4	−0.014369334	43.6933%	−0.012436634	24.3663%	−0.009371896	6.2810%	−0.009718613	2.8139%
Lab5	−0.012442583	24.4258%	−0.010901453	9.0145%	−0.010985196	9.8520%	−0.010523501	5.2350%
Lab6	−0.006108975	38.9103%	−0.008869558	11.3044%	−0.009233420	7.6658%	−0.009694310	3.0569%
		36.6605%		**13.3914%**		**6.6094%**		**2.8250%**

would improve as the time interval gets shorter. This information will become important in determining what ensemble sizes and time intervals will be suitable for numerical applications on more complex fermion systems.

Table 7 shows that for this δT range the % error decreases as the ensemble size increases. For ensemble size $m = 1000$, the avg % error is approximately 2.8%. The analogous results for a second run of the calculations (Run_2) are given in table C4 in appendix C.

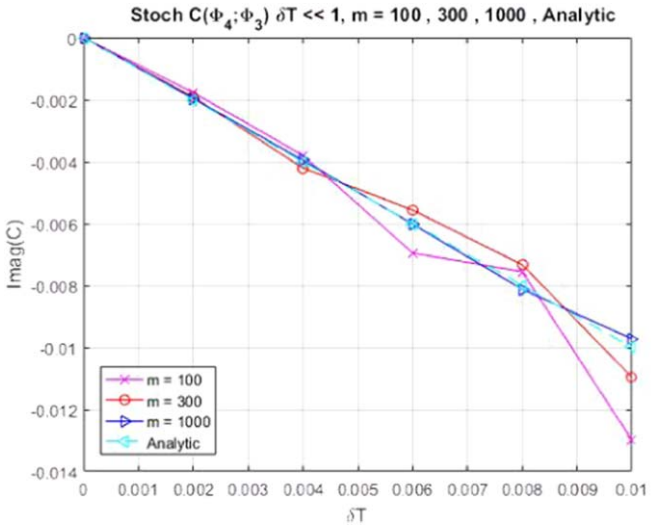

Figure 3. Figure shows the behaviour of the numerically calculated *imag*(C) and the analytic *imag*(C) versus δT for $\delta T \ll 1$. The results were obtained using the MatLab parallel processing $C(\phi_4;\phi_3)$ program for $\delta T \in [0,\ 0.01]$ and $m = 100, 300, 1000$.

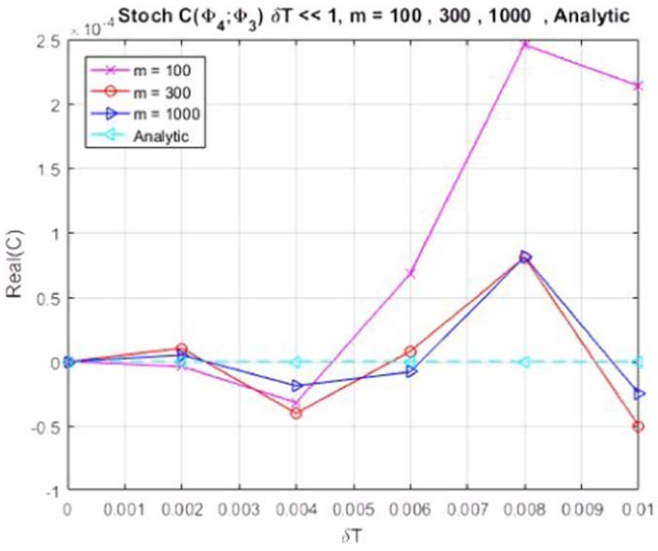

Figure 4. Figure shows the behaviour of the numerically calculated *real*(C) and the analytic *real*(C) versus δT for $\delta T \ll 1$. The results were obtained using the MatLab parallel processing $C(\phi_4;\phi_3)$ program for $\delta T \in [0,\ 0.01]$ and $m = 100, 300, 100$.

Figures 3 and 4 display the behaviour of the numerically calculated *imag*(C) and *real*(C) for various time intervals and various ensemble sizes, along with the analytic results. The time interval is small, $\delta T \ll 1$.

The two figures show that for this δT range the error decreases as the ensemble size increases. For ensemble size $m = 1000$, the stochastically calculated coherence $C(\phi_4;\phi_3)$ is in agreement with the analytic result with an average std error of approximately 4% for the two program runs made. The figures also show that the error increases as δT increases, specially for smaller ensemble sizes. The error in both *Real*(C) and *Imag*(C) are of order 10^{-4} at $\delta T \sim 0.01$ with $m = 1000$.

Figure 5 displays the results in a different way, showing the % error in $C(\phi_4;\phi_3)$ for two time intervals $\delta T = 0.01$ and $\delta T = 0.001$, but based on different ensemble sizes.

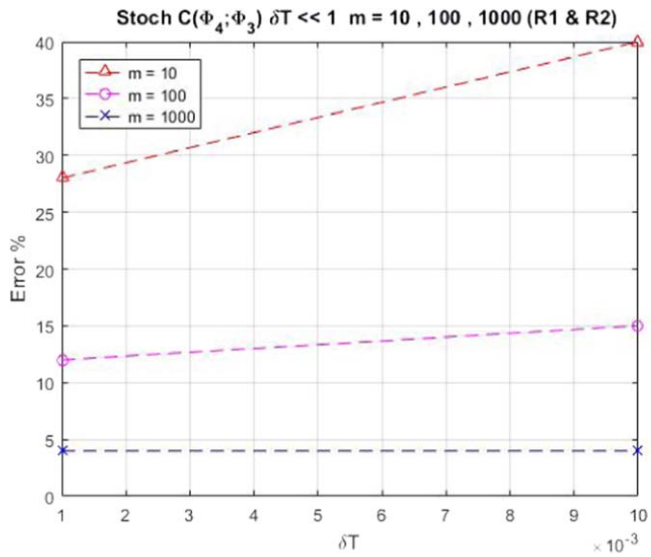

Figure 5. Figure shows the percentage error for $C(\phi_4;\phi_3)$ for different ensemble sizes m $=$ 10, 100, 1000, for $\delta T = 0.001$ and $\delta T = 0.01$.

The figure shows that for both δT values, the percentage error increases as δT increases, and it approximately scales inversely as $\sqrt{m}$ for each δT.

4.3.6. Numerical results for finite time coherence –based on 4 × 4 M for $\delta T = 0.01$

In this subsection we consider the accuracy of the numerical results for the finite time coherence for the stochastic calculations using equations (3.25) and (3.64) with ensemble size $m = 1000$ and with M 4 $\times$ 4 submatrix determined for time interval $\delta T = 0.01$.

Figures 6 and 7 display the behaviour of the numerically calculated *imag*(C) and *real*(C) for various time intervals and various ensemble sizes, along with the analytic results. The time interval is no longer small, $\delta T \sim 1$.

The two figures show that the numerically calculated coherence $C(\phi_4;\phi_3)$ based on *imag* $(M\,(16,\ 15))^n$ and *real* $(M\,(16,\ 15))^n$ is in good agreement with the analytical result. Figure 7 appears to show that the numerically calculated *real* $(M\,(16,\ 15))^n$ for the coherence though still small, is larger than expected. However the scale for

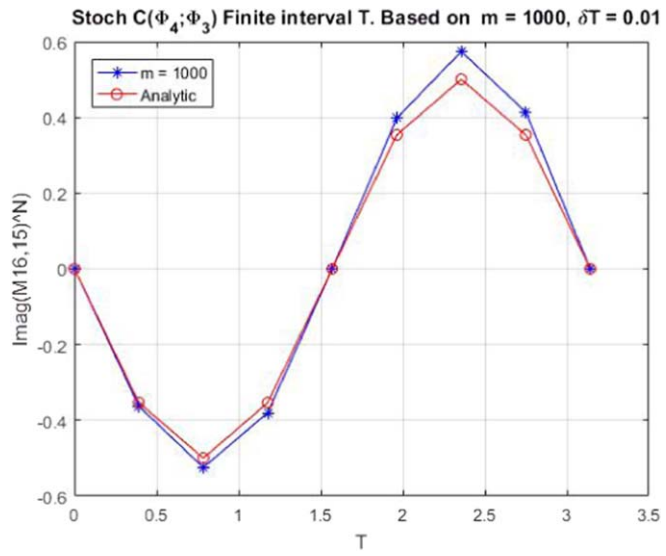

Figure 6. Figure shows the behaviour of the numerically calculated *imag* $(M\,(16,\ 15))^n$ and the analytic *imag* $(M\,(16,\ 15))^n$ versus T for the finite time calculation. The results were obtained using the MatLab parallel processing M 4 $\times$ 4 program for $\delta T = 0.01$ and $m = 1000$.

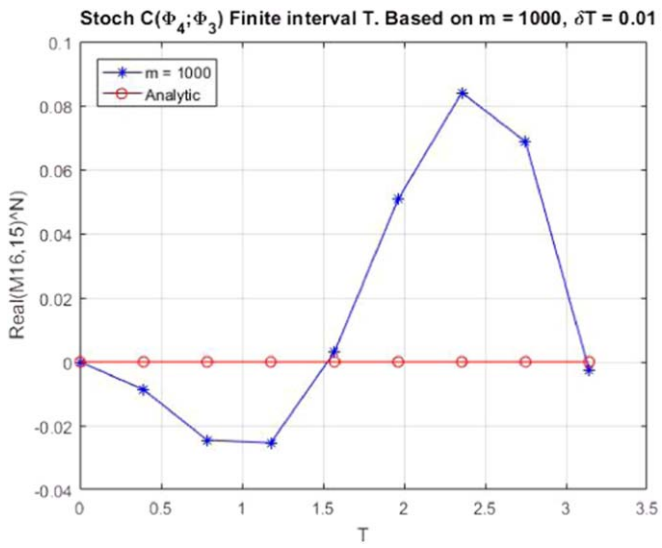

Figure 7. Figure shows the behaviour of the numerically calculated *real* $(M(16,\ 15))^n$ and the analytic *real* $(M(16,\ 15))^n$ versus T for the finite time calculation. The results were obtained using the MatLab parallel processing M 4 $\times$ 4 program for $\delta T = 0.01$ and $m = 1000$.

figure 7 is considerably smaller than that for figure 6 of *imag* $(M(16,\ 15))^n$ versus T. In both figures the difference from the analytic results is of order 0.1.

4.3.7. Conclusion about the numerical test

The four mode Cooper pair system has been treated using Grassmann phase space theory methods. The stochastic calculations for the short time behaviour and the finite time behaviour for $C(\phi_4; \phi_3)$ have been performed and have validated the approach by agreeing well with the corresponding analytic results for different choices of time interval. However, the work on this simple problem has indicated that the desk top computer (although parallel processing was used) would be inadequate for more complex calculations, and that the supercomputer facility will be needed.

5. Summary and conclusion

In this paper we have outlined the theoretical methods used in cold atom physics and described phase space theory approaches, including the recently developed Grassmann phase space theory for fermions. A brief overview of the physics for cold atom physics, focusing on the BEC/BCS crossover in Fermi gases that is of particular interest for applying Grassmann phase space theory was presented. We have set out the key equations in Grassmann phase space theory and described how numerical calculations in GPST can be carried out. We then applied GPST to a simple four mode Cooper pair model to test the validity of the stochastic approach by comparing the numerical results to the analytic results for the short and finite time behaviour of a coherence between two Fock states. In this first correct numerical application of GPST to a fermion problem, we have found the numerical stochastic calculations based on GPST and the known analytic results for the four mode Cooper pair model to be in good agreement, indicating that GPST is a valid approach. Furthermore, we have shown that GPST can be applied in stochastic calculations without the need to represent Grassmann variables on the computer. Numerical calculations are feasible because Grassmann stochastic variables at later times are related linearly to such variables at earlier times via c-number stochastic quantities. GPST should be applicable to topics involving larger numbers of modes and fermion numbers, though such application may require using a super-computer with parallel processing capabilities. Large fermion number applications could be based on using the Grassmann field version of GPST, which has also been developed (see [12, 25–27]).

Acknowledgments

The authors thank P Hannaford, H Hu, D Hicks, R Y Teh, K Ng and M Reid for helpful discussions. Help from the SUT Information Technology Centre is also acknowledged.

Appendix A. Drift, Diffusion in terms of Hamiltonian quantities

A.1. New drift, diffusion parameters $\mathscr{M}$, L

We now write (see equations (3.22), (3.23) and (3.24))

$$\mathscr{F}_{ij}^{--} = -\sum_{kl} \mathscr{M}_{ikjl}^{--} g_k g_l, \qquad \mathscr{F}_{ij}^{++} = \sum_{kl} \mathscr{M}_{ikjl}^{++} g_k^+ g_l^+, \tag{A.1}$$

$$\mathscr{F}_{ij}^{-+} = \sum_{kl} \mathscr{M}_{ikjl}^{-+} g_k g_l^+, \qquad \mathscr{F}_{ij}^{+-} = \sum_{kl} \mathscr{M}_{ikjl}^{+-} g_k^+ g_l, \tag{A.2}$$

where $\mathscr{M}^{--}$, $\mathscr{M}^{++}$, $\mathscr{M}^{-+}$ and $\mathscr{M}^{+-}$ are four $n^2 \times n^2$ c-number matrices. Also, we introduce matrices L^-, L^+ via (see equations (3.20) and (3.21))

$$A_i^- = -\sum_j L_{ij}^- g_j \qquad A_i^+ = -\sum_j L_{ij}^+ g_j. \tag{A.3}$$

A.2. Form of diffusion matrix D and drift vector A

By writing the diffusion matrix elements in the form

$$D_{pq} = \sum_{r,s=1}^{2n} Q_{rs}^{pq} g_r g_s, \tag{A.4}$$

one can see that Q is a $2n^2 \times 2n^2$ complex and symmetric matrix (from $D_{pq} = -D_{qp}$), where rows are listed as p, r and columns listed as q, s. The non-zero elements of Q can be identified from the following table

g_p	g_q	g_r	g_s	Q_{rs}^{pq}
g_i	g_j	g_k	g_l	$\mathscr{M}_{ikjl}^{--}$
g_i	g_j^+	g_k	g_l^+	$\mathscr{M}_{ikjl}^{-+}$
g_i^+	g_j	g_k^+	g_l	$\mathscr{M}_{ikjl}^{+-}$
g_i^+	g_j^+	g_k^+	g_l^+	$\mathscr{M}_{ikjl}^{++}$

From the explicit expressions in equations (3.22), (3.23), and (3.24) we see that $\mathscr{M}^{--}$, $\mathscr{M}^{++}$ are symmetric and $\mathscr{M}^{-+}$, $\mathscr{M}^{+-}$ are Hermitian.

Note that in each $n^2 \times n^2$ sub-matrix of Q, the rows p, r are in one-one correspondence with the various i, k and the columns q, s are in one-one correspondence with the various j, l. The i, k, j, l only run from $1, \ldots, n$. and $p, q, r, s = 1, \ldots, 2n$. For each row with a given form for g_p and g_q, the matrix element Q_{rs}^{pq} is given by the stated $\mathscr{M}_{ikjl}^{AB}$ when g_r and g_s are given in the same row, and zero otherwise. For example, with p and q both in the range $1, \ldots, n$ the matrix element $\mathscr{M}_{rs}^{pq}$ vanishes if either r or s is in the range $n+1, n+2, \ldots, 2n$, since $-F_{ij}^{--}$ does not involve any g_k^+ or g_l^+. Although the matrix Q could in principle have $(2n)^2$ rows and $(2n)^2$ columns, with row and column indices as the joint quantities p, r or q, s, most of the elements would be zero. Taking this into account, the matrix Q is only required to have $2n^2$ rows and $2n^2$ columns and can be formatted as

$$[Q] = \begin{bmatrix} \mathscr{M}^{--} & \mathscr{M}^{-+} \\ \mathscr{M}^{+-} & \mathscr{M}^{++} \end{bmatrix} \tag{A.5}$$

where the rows are listed in each $n^2 \times n^2$ submatrix asik and the columns are listed as jl. For each submatrix $\mathscr{M}_{ikjl}^{AB}$, specifying an element by ik (row) and jl (column) uniquely specifies the element for Q via the p_r (row) and q_s (column) indices (from the 4×4 table for Q). An example for $n = 2$ illustrates the procedure:

$p, r\downarrow, q, s \rightarrow$	11	12	21	22	33	34	43	44
11								
12								
21								
22								
33								
34								
43								
44								

(A.6)

Furthermore, by writing the drift vector in the form

$$A_p(g) = -\sum_r L_r^p g_r, \tag{A.7}$$

L is a $2n \times 2n$ c-number matrix with rows p and columns r listed as 1,2, …, $2n$. The non-zero elements of L can be identified from the following table

g_p	g_r	L_r^p
g_i	g_j	L_{ij}^-
g_i^+	g_j^+	L_{ij}^+

where $i, j = 1, \ldots, n$ and $p, r = 1, \ldots, 2n$. For each row with a given form for g_p, the matrix element L_r^p is given by the stated L_{ij}^A when g_r is given in the same row, and zero otherwise. For example, with p in the range $1, \ldots, n$ the matrix element L_r^p is zero if r is in the range $n+1, n+2, \ldots, 2n$, since $-\mathscr{C}_i^-$ does not involve any g_j^+. The matrix L has $2n$ rows and $2n$ columns, as the row and column indices are the joint quantities p and r. Thus, the matrix L may be formatted as

$$[L] = \begin{bmatrix} L^- & 0 \\ 0 & L^+ \end{bmatrix} \tag{A.8}$$

where the rows are listed in each $n \times 1$ submatrix as i and the columns are listed as j. Again, for each submatrix an element specified by$i$ (row) and j (column) can also be listed for L via p (row) and r (column), where for each submatrix ij uniquely specifies p, r. An example for $n = 2$ illustrates the procedure:

$[L] =$

$p\downarrow, r\rightarrow$	1	2	3	4
1			0	0
2			0	0
3	0	0		
4	0	0		

(A.9)

A.3. Drift Vector and diffusion matrix terms for the Cooper pair model

The drift and diffusion matrix quantities are obtained from equations (3.20) to (3.24), noting that there are no relaxation terms In terms of quantities defined in section 4.1.2 we have (see [12], p211-212)

$$\mathscr{C}_1^- = i\omega g_1 \qquad \mathscr{C}_2^- = i\omega g_2 \qquad \mathscr{C}_3^- = i\omega g_3 \qquad \mathscr{C}_4^- = i\omega g_4, \tag{A.10}$$

$$\mathscr{C}_1^+ = -i\omega g_1^+ \qquad \mathscr{C}_2^+ = -i\omega g_2^+ \qquad \mathscr{C}_3^+ = -i\omega g_3^+ \qquad \mathscr{C}_4^+ = -i\omega g_4^+. \tag{A.11}$$

$$\begin{aligned}
&\mathscr{F}_{11}^{--} = 0 \quad \mathscr{F}_{12}^{--} = \frac{\kappa}{i\hbar} g_2 g_1 \quad \mathscr{F}_{13}^{--} = 0 \quad \mathscr{F}_{14}^{--} = \frac{\kappa}{i\hbar}(g_4 g_1 + g_2 g_3), \\
&\mathscr{F}_{21}^{--} = \frac{\kappa}{i\hbar} g_1 g_2 \quad \mathscr{F}_{22}^{--} = 0 \quad \mathscr{F}_{23}^{--} = \frac{\kappa}{i\hbar}(g_3 g_2 + g_1 g_4) \quad \mathscr{F}_{24}^{--} = 0, \\
&\mathscr{F}_{31}^{--} = 0 \quad \mathscr{F}_{32}^{--} = \frac{\kappa}{i\hbar}(g_2 g_3 + g_4 g_1) \quad \mathscr{F}_{33}^{--} = 0 \quad \mathscr{F}_{34}^{--} = \frac{\kappa}{i\hbar} g_4 g_3, \\
&\mathscr{F}_{41}^{--} = \frac{\kappa}{i\hbar}(g_1 g_4 + g_3 g_2) \quad \mathscr{F}_{42}^{--} = 0 \quad \mathscr{F}_{43}^{--} = \frac{\kappa}{i\hbar} g_3 g_4 \quad \mathscr{F}_{44}^{--} = 0.
\end{aligned} \tag{A.12}$$

$$\begin{aligned}
&\mathscr{F}_{11}^{++} = 0 \quad \mathscr{F}_{12}^{++} = -\frac{\kappa}{i\hbar} g_1^+ g_2^+ \quad \mathscr{F}_{13}^{++} = 0 \quad \mathscr{F}_{14}^{++} = -\frac{\kappa}{i\hbar}(g_1^+ g_4^+ + g_3^+ g_2^+), \\
&\mathscr{F}_{21}^{++} = -\frac{\kappa}{i\hbar} g_2^+ g_1^+ \quad \mathscr{F}_{22}^{++} = 0 \quad \mathscr{F}_{23}^{++} = -\frac{\kappa}{i\hbar}(g_2^+ g_3^+ + g_4^+ g_1^+) \quad \mathscr{F}_{24}^{++} = 0, \\
&\mathscr{F}_{31}^{++} = 0 \quad \mathscr{F}_{32}^{++} = -\frac{\kappa}{i\hbar}(g_3^+ g_2^+ + g_1^+ g_4^+) \quad \mathscr{F}_{33}^{++} = 0 \quad \mathscr{F}_{34}^{++} = -\frac{\kappa}{i\hbar} g_3^+ g_4^+, \\
&\mathscr{F}_{41}^{++} = -\frac{\kappa}{i\hbar}(g_4^+ g_1^+ + g_2^+ g_3^+) \quad \mathscr{F}_{42}^{++} = 0 \quad \mathscr{F}_{43}^{++} = -\frac{\kappa}{i\hbar} g_4^+ g_3^+ \quad \mathscr{F}_{44}^{++} = 0.
\end{aligned} \tag{A.13}$$

and

$$\mathscr{F}_{ij}^{-+} = 0, \qquad \mathscr{F}_{ij}^{+-} = 0, \qquad i, j = 1, 2, 3, 4. \tag{A.14}$$

From these results the matrix elements for the sub-matrices $\mathscr{M}^{--}$, $\mathscr{M}^{++}$, $\mathscr{M}^{-+}$ and $\mathscr{M}^{+-}$ can be obtained. The results for non-zero elements are

$$\begin{aligned}
&\mathscr{M}_{1122}^{--} = \mathscr{M}_{2211}^{--} = \mathscr{M}_{1144}^{--} = \mathscr{M}_{4411}^{--} = \mathscr{M}_{3322}^{--} = \mathscr{M}_{2233}^{--} = \mathscr{M}_{3344}^{--} = \mathscr{M}_{4433}^{--} = \lambda, \\
&\mathscr{M}_{1342}^{--} = \mathscr{M}_{4213}^{--} = \mathscr{M}_{3124}^{--} = \mathscr{M}_{2431}^{--} = \lambda,
\end{aligned} \tag{A.15}$$

with

$$\lambda = \frac{\kappa}{i\hbar} \qquad \kappa = \frac{g}{V} \qquad \hbar\omega = \frac{\hbar^2\mathbf{k}^2}{2M}. \tag{A.16}$$

For the other matrices, $\mathscr{M}^{++} = (\mathscr{M}^{--})^*$ and those of the matrices $\mathscr{M}^{-+}$ and $\mathscr{M}^{+-}$ are zero. Here * means taking the complex conjugate of c-numbers. In this case, the diffusion matrix has the simple form:

$$[D] = \begin{bmatrix} -\mathscr{F}^{--} & 0 \\ 0 & +\mathscr{F}^{++} \end{bmatrix}. \tag{A.17}$$

Using these matrices the expressions for the quantities $K^p_{r,a}$ and L^p_r that specify the deterministic and noise terms in the Ito stochastic equations equation (3.47) can be determined. The details are set out in appendix sections B.1 and D.

Appendix B. List of X, M quantities for Cooper Pair Model

B.1. Specific form of the $X_{(t)}$ 36 × 1 matrix elements $\tilde{h}_x\tilde{h}_y\tilde{h}_z^+\tilde{h}_w^+$

$$\begin{aligned}
X_1 &= \overline{\tilde{h}_4\tilde{h}_3\tilde{h}_3^+\tilde{h}_4^+} & X_2 &= \overline{\tilde{h}_4\tilde{h}_3\tilde{h}_2^+\tilde{h}_4^+} & X_3 &= \overline{\tilde{h}_4\tilde{h}_3\tilde{h}_1^+\tilde{h}_4^+} \\
X_4 &= \overline{\tilde{h}_4\tilde{h}_3\tilde{h}_2^+\tilde{h}_3^+} & X_5 &= \overline{\tilde{h}_4\tilde{h}_3\tilde{h}_1^+\tilde{g}_3^+} & X_6 &= \overline{\tilde{h}_4\tilde{h}_3\tilde{h}_1^+\tilde{h}_2^+} \\
X_7 &= \overline{\tilde{h}_4\tilde{h}_2\tilde{h}_3^+\tilde{h}_4^+} & X_8 &= \overline{\tilde{h}_4\tilde{h}_2\tilde{h}_2^+\tilde{h}_4^+} & X_9 &= \overline{\tilde{h}_4\tilde{h}_2\tilde{h}_1^+\tilde{h}_4^+} \\
X_{10} &= \overline{\tilde{h}_4\tilde{h}_2\tilde{h}_2^+\tilde{h}_3^+} & X_{11} &= \overline{\tilde{h}_4\tilde{h}_2\tilde{h}_1^+\tilde{h}_3^+} & X_{12} &= \overline{\tilde{h}_4\tilde{h}_2\tilde{h}_1^+\tilde{h}_2^+} \\
X_{13} &= \overline{\tilde{h}_4\tilde{h}_1\tilde{h}_3^+\tilde{h}_4^+} & X_{14} &= \overline{\tilde{h}_4\tilde{h}_1\tilde{h}_2^+\tilde{h}_4^+} & X_{15} &= \overline{\tilde{h}_4\tilde{h}_1\tilde{h}_1^+\tilde{h}_4^+} \\
X_{16} &= \overline{\tilde{h}_4\tilde{h}_1\tilde{h}_2^+\tilde{h}_3^+} & X_{17} &= \overline{\tilde{h}_4\tilde{h}_1\tilde{h}_1^+\tilde{h}_3^+} & X_{18} &= \overline{\tilde{h}_4\tilde{h}_1\tilde{h}_1^+\tilde{h}_2^+} \\
X_{19} &= \overline{\tilde{h}_3\tilde{h}_2\tilde{h}_3^+\tilde{h}_4^+} & X_{20} &= \overline{\tilde{h}_3\tilde{h}_2\tilde{h}_2^+\tilde{h}_4^+} & X_{21} &= \overline{\tilde{h}_3\tilde{h}_2\tilde{h}_1^+\tilde{h}_4^+} \\
X_{22} &= \overline{\tilde{h}_3\tilde{h}_2\tilde{h}_2^+\tilde{h}_3^+} & X_{23} &= \overline{\tilde{h}_3\tilde{h}_2\tilde{h}_1^+\tilde{h}_3^+} & X_{24} &= \overline{\tilde{h}_3\tilde{h}_2\tilde{h}_1^+\tilde{h}_2^+} \\
X_{25} &= \overline{\tilde{h}_3\tilde{h}_1\tilde{h}_3^+\tilde{h}_4^+} & X_{26} &= \overline{\tilde{h}_3\tilde{h}_1\tilde{h}_2^+\tilde{h}_4^+} & X_{27} &= \overline{\tilde{h}_3\tilde{h}_1\tilde{h}_1^+\tilde{h}_4^+} \\
X_{28} &= \overline{\tilde{h}_3\tilde{h}_1\tilde{h}_2^+\tilde{h}_3^+} & X_{29} &= \overline{\tilde{h}_3\tilde{h}_1\tilde{h}_1^+\tilde{h}_3^+} & X_{30} &= \overline{\tilde{h}_3\tilde{h}_1\tilde{h}_1^+\tilde{h}_2^+} \\
X_{31} &= \overline{\tilde{h}_2\tilde{h}_1\tilde{h}_3^+\tilde{h}_4^+} & X_{32} &= \overline{\tilde{h}_2\tilde{h}_1\tilde{h}_2^+\tilde{h}_4^+} & X_{33} &= \overline{\tilde{h}_2\tilde{h}_1\tilde{h}_1^+\tilde{h}_4^+} \\
X_{34} &= \overline{\tilde{h}_2\tilde{h}_1\tilde{h}_2^+\tilde{h}_3^+} & X_{35} &= \overline{\tilde{h}_2\tilde{h}_1\tilde{h}_1^+\tilde{h}_3^+} & X_{36} &= \overline{\tilde{h}_2\tilde{h}_1\tilde{h}_1^+\tilde{h}_2^+}.
\end{aligned} \tag{B.1}$$

B.2. List of elements $\Theta^-_{\alpha_1,\beta_1}\Theta^-_{\alpha_2,\beta_2}\Theta^+_{\alpha_3,\beta_3}\Theta^+_{\alpha_4,\beta_4}$ of first row for $M_{\alpha,\beta}$ 36 × 36 matrix

$$\begin{aligned}
M_{1,1} &= \overline{\Theta^-_{4,4}\Theta^-_{3,3}\Theta^+_{3,3}\Theta^+_{4,4}} & M_{1,2} &= 0 & M_{1,3} &= \overline{\Theta^-_{4,4}\Theta^-_{3,3}\Theta^+_{3,1}\Theta^+_{4,4}} \\
M_{1,4} &= (-1)\overline{\Theta^-_{4,4}\Theta^-_{3,3}\Theta^+_{3,3}\Theta^+_{4,2}} & M_{1,5} &= 0 & M_{1,6} &= \overline{\Theta^-_{4,4}\Theta^-_{3,3}\Theta^+_{3,1}\Theta^+_{4,2}} \\
M_{1,7} &= 0 & M_{1,8} &= 0 & M_{1,9} &= 0 \\
M_{1,10} &= 0 & M_{1,11} &= 0 & M_{1,12} &= 0 \\
M_{1,13} &= \overline{\Theta^-_{4,4}\Theta^-_{3,1}\Theta^+_{3,3}\Theta^+_{4,4}} & M_{1,14} &= 0 & M_{1,15} &= \overline{\Theta^-_{4,4}\Theta^-_{3,1}\Theta^+_{3,1}\Theta^+_{4,4}} \\
M_{1,16} &= (-1)\overline{\Theta^-_{4,4}\Theta^-_{3,1}\Theta^+_{3,3}\Theta^+_{4,2}} & M_{1,17} &= 0 & M_{1,18} &= \overline{\Theta^-_{4,4}\Theta^-_{3,1}\Theta^+_{3,1}\Theta^+_{4,2}} \\
M_{1,19} &= (-1)\overline{\Theta^-_{4,2}\Theta^-_{3,3}\Theta^+_{3,3}\Theta^+_{4,4}} & M_{1,20} &= 0 & M_{1,21} &= (-1)\overline{\Theta^-_{4,2}\Theta^-_{3,3}\Theta^+_{3,1}\Theta^+_{4,4}} \\
M_{1,22} &= (-1)(-1)\overline{\Theta^-_{4,2}\Theta^-_{3,3}\Theta^+_{3,3}\Theta^+_{4,2}} & M_{1,23} &= 0 & M_{1,24} &= (-1)\overline{\Theta^-_{4,2}\Theta^-_{3,3}\Theta^+_{3,1}\Theta^+_{4,2}} \\
M_{1,25} &= 0 & M_{1,26} &= 0 & M_{1,27} &= 0 \\
M_{1,28} &= 0 & M_{1,29} &= 0 & M_{1,30} &= 0 \\
M_{1,31} &= \overline{\Theta^-_{4,2}\Theta^-_{3,1}\Theta^+_{3,3}\Theta^+_{4,4}} & M_{1,32} &= 0 & M_{1,33} &= \overline{\Theta^-_{4,2}\Theta^-_{3,1}\Theta^+_{3,1}\Theta^+_{4,4}} \\
M_{1,34} &= (-1)\overline{\Theta^-_{4,2}\Theta^-_{3,1}\Theta^+_{3,3}\Theta^+_{4,2}} & M_{1,35} &= 0 & M_{1,36} &= \overline{\Theta^-_{4,2}\Theta^-_{3,1}\Theta^+_{3,1}\Theta^+_{4,2}}.
\end{aligned} \tag{B.2}$$

Note that some elements of $M(\alpha,\beta)$ are zero because one or more of the $\Theta^{\pm}$ involved is actually zero.

For the second row of $M_{\alpha,\beta}$ $(M_{2,1} - M_{2,36})$ the first sub-indices of the Θs product terms will be changed from 4, 3, 3, 4 in $\Theta^-_{4,\beta_1}\Theta^-_{3,\beta_2}\Theta^+_{3,\beta_3}\Theta^+_{4,\beta_4}$ to 4, 3, 2, 4 i.e. $\Theta^-_{4,\beta_1}\Theta^-_{3,\beta_2}\Theta^+_{2,\beta_3}\Theta^+_{4,\beta_4}$ and will be fixed for the entire row, with

the second sub-indices namely (β_1, β_2, β_3,β_4) having the same combinations as those of row 1 (for all row 2 elements). By the same token for the third row ($M_{3,1} - M_{3,36}$), the first sub_indices of the Θ *s* product terms will be changed for the entire row to be $\Theta^-_{4,\beta_1}\Theta^-_{3,\beta_2}\Theta^+_{1,\beta_3}\Theta^+_{4,\beta_4}$ with the second sub-indices (β_1, β_2, β_3,β_4) combinations being the same as those of rows 1 and 2 (for all row 3 elements). It is to be noted that only the first sub-indices α of $M_{\alpha,\beta}$ are changing across the various rows, while it has one fixed combination for each row, while the second sub-indices β combinations of $M_{\alpha,\beta}$ are varying from one element to the next across the same row, but these combinations are the same across the various rows.

To construct the $M_{\alpha,\beta}$ various rows, then for each row we take as the first sub-indices α combination in the Θ product ($\Theta^-_{\alpha_1,\beta_1}\Theta^-_{\alpha_2,\beta_2}\Theta^+_{\alpha_3,\beta_3}\Theta^+_{\alpha_4,\beta_4}$), one of the of the Grassmann variable's product combinations (x, y, z, w) of the $X_{(t)}$ matrix. Therefore for row 1, $\alpha_1 = 4, \alpha_2 = 3, \alpha_3 = 3, \alpha_4 = 4$ while for row 2, $\alpha_1 = 4, \alpha_2 = 3, \alpha_3 = 2$, $\alpha_4 = 4$ and so on. For each row the α combination ($\alpha_1\alpha_2\alpha_3\alpha_4$) is fixed across the entire row. For each row we then combine the fixed first sub-indices ($\alpha_1\alpha_2\alpha_3\alpha_4$) combination with each one of the 36 Grassmann variable's product combinations (x, y, z, w) of the $X_{(t)}$ matrix. These will form the second sub-indices β combinations in ($\Theta^-_{\alpha_1,\beta_1}\Theta^-_{\alpha_2,\beta_2}\Theta^+_{\alpha_3,\beta_3}\Theta^+_{\alpha_4,\beta_4}$), of the Θ *s* product namely ($\beta_1\beta_2\beta_3\beta_4$).

To summarize, the α combination is fixed for the same row but varies from one row to the next, while the β combinations vary from one row element to the next, However these combinations are the same for various $M_{\alpha,\beta}$ rows.

Within this arrangement, and upon mapping the $X_{(t+\delta t)}$ indices to the first set of sub-indices α of $\boldsymbol{M_{\alpha,\beta}}$ (r, s, v, $u \rightarrow \alpha$) and the $X_{(t)}$ indices to the second set of sub-indices β of $M_{\alpha,\beta}$(x, y, z, $w \rightarrow \beta$) for the first step, one finds that the $X_{(t+\delta t)}$ matrix will have the same Grassmann variable combinations as that of the $X_{(t)}$ matrix.

An analogous approach is applied to treat the columns of M.

Appendix C. Evaluation of stochastic averages

C.1. Analytic evaluation of the elements $M(15,\ 15)$, $M(21,\ 15)$, $M(22,\ 15)$, $M(36,\ 15)$ of column 15

$$\begin{aligned} M(15,\ 15) &= (+1)\overline{\Theta^-_{4,4}\Theta^-_{1,1}\Theta^+_{1,1}\Theta^+_{4,4}}. \\ &= (-1)\Bigg[\left(1 + \frac{1}{\sqrt{2i}}(\delta\widetilde{\Omega}_6 + \delta\widetilde{\Omega}_{16})\right)\left(1 + \frac{1}{\sqrt{2i}}(\delta\widetilde{\Omega}_1 + \delta\widetilde{\Omega}_{11})\right) \\ &\quad \times \left(1 + \frac{1}{(\sqrt{2i})^*}(\delta\widetilde{\Omega}^+_1 + \delta\widetilde{\Omega}^+_{11})\right)\left(1 + \frac{1}{(\sqrt{2i})^*}(\delta\widetilde{\Omega}^+_6 + \delta\widetilde{\Omega}^+_{16})\right)\Bigg]_{StochAvg} \\ &= 1. \end{aligned} \tag{C.1}$$

Here terms include stochastic average of products of zero, one, two, three, four $\delta\widetilde{\Omega}s$, but no two $\delta\widetilde{\Omega}s$ are the same, so only the products just involving 1 contribute.

$$\begin{aligned} M(21,\ 15) &= (-1)\overline{\Theta^-_{3,1}\Theta^-_{2,4}\Theta^+_{1,1}\Theta^+_{4,4}}. \\ &= (-1)\Bigg[\left(\frac{1}{\sqrt{2i}}(\delta\widetilde{\Omega}_8 + \delta\widetilde{\Omega}_9)\right)\left(\frac{1}{\sqrt{2i}}(\delta\widetilde{\Omega}_8 + \delta\widetilde{\Omega}_9)\right) \\ &\quad \times \left(1 + \frac{1}{(\sqrt{2i})^*}(\delta\widetilde{\Omega}^+_1 + \delta\widetilde{\Omega}^+_{11})\right)\left(1 + \frac{1}{(\sqrt{2i})^*}(\delta\widetilde{\Omega}^+_6 + \delta\widetilde{\Omega}^+_{16})\right)\Bigg]_{StochAvg} \\ &= (-1)\left(\frac{1}{(\sqrt{2i})}\right)^2\overline{(\delta\widetilde{\Omega}_8 + \delta\widetilde{\Omega}_9)(\delta\widetilde{\Omega}_8 + \delta\widetilde{\Omega}_9)} \\ &= (-1)\frac{1}{(2i)}(\overline{(\delta\widetilde{\Omega}_8)^2} + \overline{(\delta\widetilde{\Omega}_9)^2}) \\ &= (-1)\frac{1}{2i}(\delta T + \delta T) \\ &= -\frac{1}{i}(\delta T). \end{aligned} \tag{C.2}$$

$$
\begin{aligned}
M(22,\,15) &= (+1)\overline{\Theta^{-}_{3,1}\Theta^{-}_{2,4}\Theta^{+}_{2,4}\Theta^{+}_{3,1}}.\\
&= \left[\left(\frac{1}{\sqrt{2i}}(\delta\widetilde{\Omega}_8+\delta\widetilde{\Omega}_9)\right)\left(\frac{1}{\sqrt{2i}}(\delta\widetilde{\Omega}_8+\delta\widetilde{\Omega}_9)\right)\right.\\
&\quad\left.\times\left(\frac{1}{(\sqrt{2i})^*}(\delta\widetilde{\Omega}^{+}_8+\delta\widetilde{\Omega}^{+}_9)\right)\left(\frac{1}{(\sqrt{2i})^*}(\delta\widetilde{\Omega}^{+}_8+\delta\widetilde{\Omega}^{+}_9)\right)\right]_{StochAvg}\\
&= \left(\frac{1}{(\sqrt{2i})}\right)^2\left(\frac{1}{(\sqrt{2i})^*}\right)^2\overline{(\delta\widetilde{\Omega}^{2}_8\cdot\delta\widetilde{\Omega}^{+2}_8)}+\overline{(\delta\widetilde{\Omega}^{2}_8\cdot\delta\widetilde{\Omega}^{+2}_9)}+\overline{(\delta\widetilde{\Omega}^{2}_9\cdot\delta\widetilde{\Omega}^{+2}_8)}+\overline{(\delta\widetilde{\Omega}^{2}_9\cdot\delta\widetilde{\Omega}^{+2}_9)}\\
&= \frac{1}{2i}\frac{1}{(2i)^*}(\overline{(\delta\widetilde{\Omega}_8)^2}\cdot\overline{(\delta\widetilde{\Omega}^{+}_8)^2}+\overline{(\delta\widetilde{\Omega}_8)^2}\cdot\overline{(\delta\widetilde{\Omega}^{+}_9)^2}+\overline{(\delta\widetilde{\Omega}_9)^2}\cdot\overline{(\delta\widetilde{\Omega}^{+}_8)^2}+\overline{(\delta\widetilde{\Omega}_9)^2}\cdot\overline{(\delta\widetilde{\Omega}^{+}_9)^2})\\
&= \frac{1}{4}((\delta T)^2+(\delta T)^2+(\delta T)^2+(\delta T)^2)\\
&= (\delta T)^2.
\end{aligned}
\tag{C.3}
$$

$$
\begin{aligned}
M(36,\,15) &= \overline{\Theta^{-}_{2,4}\Theta^{-}_{1,1}\Theta^{+}_{1,1}\Theta^{+}_{2,4}}.\\
&= \left[\left(\frac{1}{\sqrt{2i}}(\delta\widetilde{\Omega}_8+\delta\widetilde{\Omega}_9)\right)\left(1+\frac{1}{\sqrt{2i}}(\delta\widetilde{\Omega}_1+\delta\widetilde{\Omega}_{11})\right)\right.\\
&\quad\left.\times\left(1+\frac{1}{(\sqrt{2i})^*}(\delta\widetilde{\Omega}^{+}_1+\delta\widetilde{\Omega}^{+}_{11})\right)\left(\frac{1}{(\sqrt{2i})^*}(\delta\widetilde{\Omega}^{+}_8+\delta\widetilde{\Omega}^{+}_9)\right)\right]_{StochAvg}\\
&= 0.
\end{aligned}
\tag{C.4}
$$

Terms include the stochastic average of products of two, three, four $\delta\widetilde{\Omega}s$, but no two $\delta\widetilde{\Omega}s$ are the same, so all products give zero.

C.2. Rows 16, 21, 22 for matrix M 4 × 4 submatrix

Table C1. Table shows the numerical results for the imag and real parts of $M(16,\,15)$, $M(16,\,16)$, $M(16,\,21)$, $M(16,\,22)$ across the 6 parallel processing labs. The results were obtained using the MatLab parallel processing program for M 4 × 4 matrix. The average matrix element, the average error and the σ error are also shown for each of these matrix elements.

M(Alpha,Beta) Row 16

PP _Run_1 m = 1000	δT = 0.01							
	M(16, 15) $(-44\_11\_24\_31)_{Stoch}$		M(16, 16) $(44\_11\_22\_33)_{Stoch}$		M(16, 21) $(42\_13\_24\_31)_{Stoch}$		M(16, 22) $(-42\_13\_22\_33)_{Stoch}$	
	Real	Img	Real	Img	Real	Img	Real	Img
Lab1	0.000026125	−0.010445811	0.994628272	−0.001412707	0.000123437	+0.000000000	0.000139789	+0.010152874
Lab2	−0.000137482	−0.009766178	1.003941551	+0.000283385	0.000103457	+0.000000000	−0.000091416	+0.010813706
Lab3	0.000095509	−0.009903980	0.998606186	−0.002130266	0.000101516	+0.000000000	0.000100779	+0.010239848
Lab4	−0.000005378	−0.009606351	1.004606801	+0.001032299	0.000090849	+0.000000000	−0.000047954	+0.010520640
Lab5	−0.000030777	−0.010522694	1.002122085	−0.000282594	0.000110022	+0.000000000	0.000094503	+0.009805886
Lab6	−0.000019709	−0.009863232	0.999249308	−0.001128745	0.000118588	+0.000000000	−0.000083637	+0.010706543
Avg_Value	−0.000011952 −0.01001804i		1.0005257 −0.000606438i		1.0797816e−04		0.00001867733 + 0.010373249i	
Avg Error %		3.0479	0.3031		11.0285			4.3795
σ Error %		3.4388	0.3479		13.4984			5.0842

Table C2. Table shows the numerical results for the imag and real parts of $M(21,15)$, $M(21,16)$, $M(21,21)$, $M(21,22)$ across the 6 parallel processing labs. The results were obtained using the MatLab parallel processing program for $M\,4 \times 4$ matrix. The average matrix element, the average error and the σ error are also shown for each of these matrix elements.

M(Alpha,Beta) Row 21

PP _Run_1 m = 1000	δT = 0.01							
	M(21, 15) $(-31\_24\_11\_44)_{Stoch}$		M(21, 16) $(31\_24\_13\_42)_{Stoch}$		M(21, 21) $(33\_22\_11\_44)_{Stoch}$		M(21, 22) $(-33\_22\_13\_42)_{Stoch}$	
	Real	Img	Real	Img	Real	Img	Real	Img
Lab1	−0.000005239	+0.009514253	0.000098798	+0.000000000	0.994628272	−0.001412707	−0.000035235	−0.010266260
Lab2	0.000064844	+0.009720117	0.000092853	+0.000000000	1.003941551	+0.000283385	0.000015882	−0.009033418
Lab3	0.000047470	+0.009835592	0.000103716	+0.000000000	0.998606186	−0.002130266	−0.000005336	−0.010379494
Lab4	−0.000033554	+0.009897884	0.000096877	+0.000000000	1.004606801	+0.001032299	−0.000062297	−0.010062040
Lab5	0.000048607	+0.009217449	0.000083007	+0.000000000	1.002122085	−0.000282594	0.000030534-	−0.009314542
Lab6	0.000047068	+0.009736277	0.000102945	+0.000000000	0.999249308	−0.001128745	−0.000020466	−0.010934714
Avg_Value	0.00002819933 + 0.00965359i		9.636599e−05		1.0005257 −0.000606438i		−0.00001281966	−0.0099984113i
Avg Error %		3.4640	5.8543		0.3031			5.4909
σ Error %		4.1507	7.8901		0.3479			6.4506

Table C3. Table shows the numerical results for the imag and real parts of $M(22,15)$, $M(22,16)$, $M(22,21)$, $M(22,22)$ across the 6 parallel processing labs. The results were obtained using the MatLab parallel processing program for $M\,4 \times 4$ matrix. The average matrix element, the average error and the σ error are also shown for each of these matrix elements.

M(Alpha,Beta) Row 22

PP _Run_1 m = 1000	δT = 0.01							
	M(22, 15) $(31\_24\_24\_31)_{Stoch}$		M(22, 16) $(-31\_24\_22\_33)_{Stoch}$		M(22, 21) $(-33\_22\_24\_31)_{Stoch}$		M(22, 22) $(33\_22\_22\_33)_{Stoch}$	
	Real	Img	Real	Img	Real	Img	Real	Img
Lab1	0.000098249	+0.000000000	−0.000005239	+0.009514253	0.000026125	−0.010445811	0.994628272	−0.001412707
Lab2	0.000104835	+0.000000000	0.000064844	+0.009720117	−0.000137482	−0.009766178	1.003941551	+0.000283385
Lab3	0.000113925	+0.000000000	0.000047470	+0.009835592	0.000095509	−0.009903980	0.998606186	−0.002130266
Lab4	0.000089835	+0.000000000	−0.000033554	+0.009897884	−0.000005378	−0.009606351	1.004606801	+0.001032299
Lab5	0.000098447	+0.000000000	0.000048607	+0.009217449	−0.000030777	−0.010522694	1.002122085	−0.000282594
Lab6	0.000116991	+0.000000000	0.000047068	+0.009736277	−0.000019709	−0.009863232	0.999249308	−0.001128745
Avg_Value	1.0371366e−04		0.00002819933 + 0.00965359i		−0.000011952 −0.010018041i		1.0005257005	−0.000606438i
Avg Error %	8.2033			3.4640		3.0479	0.3031	
σ Error %	10.1224			4.1507		3.4388	0.3479	

C.3. Symmetry considerations

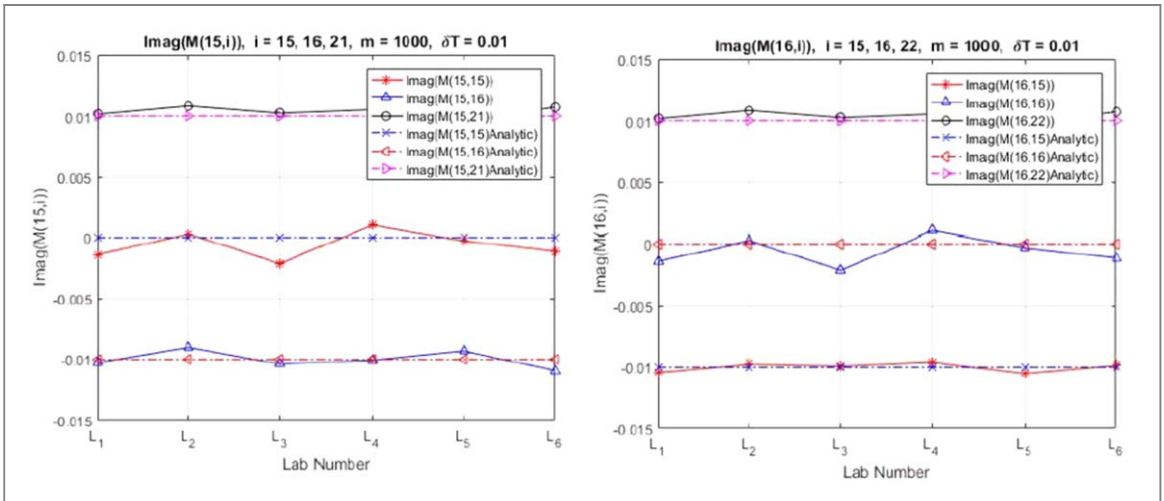

Figure C1. Figure displays clearly the symmetry between the various elements of the $M\,4 \times 4$ submatrix.

In Figure C1 note that for the first two plots (for $img(15, i)$ where $i = 15, 16, 22$)), the curves for the stochastic average points for $M(15, 15)$ coincide exactly with that for $M(16, 16)$ and that for $M(15, 21)$ coincide exactly with that for $M(16, 22)$. This is because in the table of results file, the values in Column 1 of the first table (for row 15) are identical to those in column 2 of the second table (for row 16). Similarly, the values in Column 3 of the first table (for row 15), are exactly the same as those in column 4 of the second table (for row 16). This, in turn, is due to the fact that the Θ product combinations for the elements $M(15, 15)$ [44111144] and $M(16, 16)$ [44112233] (and for $M(15, 21)$ [−42131144] and $M(16, 22)$ [−42132233]) although not exactly the same, yet they yield the same results when their relevant Θ products are multiplied (same brackets of delta Wiener combinations but in a different order. Similar arguments hold for the two plots for $img(21, i)$ where $i = 15, 21, 22$ and $img(22, i)$ with $i = 16, 21, 22$.

In other words and to be more precise: for each of Labs 1, 2, ..,6 there are 1000 choices made (by MatLab) for each of the 16 independent Wiener increments $\delta\widetilde{\Omega}_1$, $\delta\widetilde{\Omega}_{11}$, $\delta\widetilde{\Omega}_3$, $\delta\widetilde{\Omega}_{14}$, $\delta\widetilde{\Omega}_6$, $\delta\widetilde{\Omega}_{16}$,$\delta\widetilde{\Omega}_8$, $\delta\widetilde{\Omega}_9$ and $\delta\widetilde{\Omega}_1^+$, $\delta\widetilde{\Omega}_{11}^+$,$\delta\widetilde{\Omega}_3^+$, $\delta\widetilde{\Omega}_{14}^+$, $\delta\widetilde{\Omega}_6^+$, $\delta\widetilde{\Omega}_{16}^+$, $\delta\widetilde{\Omega}_8^+$, $\delta\widetilde{\Omega}_9^+$ and the result for each specific element of the 4×4 matrix M calculated using equation (3.47). These are then averaged to give the stochastic value for the matrix element. For different Labs, the 1000 choices of the 16 Wiener increments will be different, hence the 6 independent (and different) results for each specific element of M shown in tables 1 and C1–C3. The average of these for the 6 Labs is also quoted in tables 1 and C1–C3 , and amount to determining the stochastic averages for an ensemble size of $m = 6 \times 1000 = 6000$. It will be noticed that the results for the 6 Labs for certain pairs of matrix elements are the same—for example $M(15, 21)$ and $M(16, 22)$. This is because the most important pairs of Wiener increments are the same –for example $M(15, 21)$ and $M(16, 22)$ both involve $(\delta\widetilde{\Omega}_3 + \delta\widetilde{\Omega}_{14})$ twice, both arising from the same off-diagonal Θ matrix elements $\Theta^-_{(4,2)}$ and $\Theta^-_{(1,3)}$. Other pairs of Wiener increments arising from diagonal matrix elements $\Theta^-_{(1,1)}$ and $\Theta^-_{(4,4)}$ or $\Theta^-_{(2,2)}$ and $\Theta^-_{(3,3)}$ make negligible difference, since the leading terms in these elements are order 1 (rather than order $\sqrt{\delta T}$). The stochastic averaging process determines each 4×4 element to an accuracy of ca 4% for the effective ensemble sizes of 6000 independent calculations. The accuracy is specified by the standard deviation of the results in the 6 Labs from the theoretical value for the matrix element as shown in tables 1 and C1–C3

C.4. Results for Run 2 for the short time behaviour parallel processing program

Table C4. Table shows the std error for the numerically calculated $imag(C)$ across the 6 parallel processing labs, for $\delta T \ll 1$. The results were obtained in run 2 for the MatLab parallel processing $C(\phi_4; \phi_3)$ program for $\delta T \in [0,0.01]$ and $m = 100, 300, 1000$.

The percentage error tables for C(Φ4; Φ3), M = 10, 100, 300, 1000 for δT = 0.01 R2

PP _Run_2	δT = 0.01							
	M = 10		M = 100		M = 300		M = 1000	
	Img(C)	Std_Error	Img(C)	Std_Error	Img(C)	Std_Error	Img(C)	Std_Error
Lab1	−0.020201025	102.0103%	−0.010825259	8.2526%	−0.011142919	11.4292%	−0.010656032	6.5603%
Lab2	−0.009525434	4.7457%	−0.008632182	13.6782%	−0.009663882	3.3612%	−0.009799356	2.0064%
Lab3	−0.011987390	19.8739%	−0.011510730	15.1073%	−0.011623230	16.2323%	−0.010633817	6.3382%
Lab4	−0.015575553	55.7555%	−0.014368173	43.6817%	−0.011090911	10.9091%	−0.010480200	4.8020%
Lab5	−0.005507118	44.9288%	−0.009222784	7.7722%	−0.011276930	12.7693%	−0.010733943	7.3394%
Lab6	−0.012701387	27.0139%	−0.011184569	11.8457%	−0.011949510i	19.4951%	−0.010660227i	6.6023%
		42.3880%		**16.7229%**		**12.3660%**		**5.6081%**

Table C4 shows that for this δT range the std error decreases as the ensemble size increases. For ensemble size $m = 1000$, the avg std error is approximately 5.6%.

Appendix D. Programming considerations

D.1. Parallel Processing in MatLab - an overview

Parallel Computing entails the use of two or more processors in combination to solve a single problem. Serial performance improvements have slowed, while parallel hardware has become ubiquitous. On the other hand, Parallel programs are typically harder to write and debug than serial programs. Parallel speedup is a function of the number of cores where $speedup(p) = \frac{time_{old}}{time_{new}(cores)}$ where p is the number of cores.

MATLAB Parallel Computing Toolbox supports three types of parallelism. The one suited to a single computer with multiple cores is *Multithreaded parallelism*, where one instance of MATLAB automatically

generates multiple simultaneous instruction streams. Multiple processors or cores, sharing the memory of a single computer, execute these streams. To make use of that concept we certain commands must be employed within the source code. The process starts by opening a MATLAB pool, this is done using the 'parpool' command which creates workers (or labs) to do parallel computations. On the i7 processor at SUT there are 6 cores. The parpool commnad creates 6 labs A client and 5 normal labs (or workers) one equivalent to each core present. The client is the head MATLAB session –creates workers, distributes work, receives results. The Workers/Labs are independent, headless, MATLAB sessions. They do not share memory, and are created before being used and destroyed after the program execution takes its course.

To make use of multithreaded parallelism, one uses the SPMD (single program multiple data). This command explicitly and/or automatically divide work and data between workers/labs and communicate between workers/labs. The data created before the SPMD block is copied to all workers, whereas the data created within the SPMD block, is unique to worker, composite on client. Memory is not shared by the workers. Data can be shared between workers using special data types: composite, distributed, codistributed. The parallel processing toolbox also contains parallel for loop constructs and commands for tall arrays manipulation where the processing for such arrays is distributed among the available workers with respect to their rows or columns.

D.1.1. The M 36 × 36 matrix program description

At its first stage the program lists the $\Theta^{-}$and Θ^{+} four products forming the 1296 elements of $M_{Prelim}(\alpha, \beta)$. At its second stage, the second indices permutations for the $\Theta^{-}$and Θ^{+} four products of $M_{Prelim}(\alpha, \beta)$ are correctly performed. At the third stage the program makes use of an additional module to populate the $M_{Prelim}(\alpha, \beta)$ matrix with the values of the Θ^{-} and Θ^{+} products of the surviving elements. This takes place after performing the second indices permutations, to form the $M_{PreStochastic}(\alpha, \beta)$ matrix. The population process involves inspecting the digits corresponding to the $\Theta^{-}$and Θ^{+}products of each of the surviving elements, where the program converts those digits to strings. For example, the digits accompanied with a minus sign forming the element M (16,15), namely: (−)44112431 indicates that it is composed of the $\{\Theta^{-}_{4,4}\Theta^{-}_{1,1}\Theta^{+}_{2,4}\Theta^{+}_{3,1}\}$ product with a minus sign. After considering the minus sign, the program converts 44112431 to a string, separates each two characters of the resulting string, and then using iterative and conditional statements constructs (for loops and if statements), it inspects the digital content of each two characters of the separated string successively. The program then creates numeric variables with names relevant to the digital content of each couple of separated characters of the original string, and gives values to those variables. Hence the variable 44 is assigned the value of $\Theta^{-}_{4,4}$, 11 the value of $\Theta^{-}_{1,1}$... etc. At the final stage the program calculates the stochastic average for each of the $M_{PreStochastic}(\alpha, \beta)$ elements, to form the $M(\alpha, \beta)$ matrix for each member i of the ensemble where $i = 1,2, \ldots, m$. The program writes its intermediate steps and final output results to a file.

D.1.2. Parallel Processing program for the M 4 × 4 submatrix –evaluating rows 15, 16, 21, 22 –programming issues

After knowing the form and all the analytic values for the elements of the $M(\alpha, \beta)$ 36 × 36 matrix, a program was coded to perform the numerical calculation and confirm stochastically the analytic values of the M matrix elements of rows 15, 16, 21 and 22, namely: $M(i, j)$ where $i, j = 15, 16, 21, 22$.

To test the finite time behaviour and compare the numerical results with the analytical ones, a parallel processing program was written to calculate the stochastic average of $C(\varphi_4; \varphi_3)$ for $\delta T \gtrsim 1$. Initially the program employed the $M(\alpha, \beta)$ 36 × 36 matrix, which was to be multiplied successively to obtain the stochastic average of $(M(16, 15))^n$, where $T = n\delta T$. A considerable processing time was noted, as the program was evaluating all the 1296 elements of the 36 × 36 M matrix for each member i of the ensemble. It then displayed the stochastic averages of all the M elements in files (which included the above mentioned 16 elements of Rows 15, 16, 21 and 22). Performing the calculation in that manner had proven to be extremely taxing in terms of complexity and computer processing time. For example, even with the parallel processing capability utilized, only 10 members of the ensemble were processed per hour. At this rate, it would have taken the program 4 days to process1000 ensemble members. Since the elements of Rows 15, 16, 21 and 22 are the main elements relevant to the coherences and populations of the $|\phi_4\rangle$ and $|\phi_3\rangle$ states, a simpler parallel processing program was later developed with the aim of reducing the processing time relevant to the initial $C(\varphi_4; \varphi_3)$ for $\delta T \gtrsim 1$ program: This modified program concentrated only on the 16 elements of the $M(4 \times 4)$, and was used to confirm the analytic values of this submatrix for $\delta T = 0.01$, and then to calculate the finite time behaviour for element $M(16,15)$. The process began by calculating the stochastic average values for all the matrix elements of the M 4 × 4 submatrix, across the 6 labs available, and then evaluating the average matrix element for each of the elements. The resulting numerical M was found to be not quite complex symmetric as was the case with its analytic counterpart. One then had to resort to biorthogonality to calculate the required finite time behaviour of the coherence $C(\phi_4; \phi_3)$ from the final stochastic results for the 4 × 4 matrix M with $\delta T = 0.01$. The calculation was quite informative, as its results indicated that the stochastic approach does confirm the analytic result for the finite time behaviour of $C(\phi_4; \phi_3)$ given by equation (4.41) (see also equation(3.65)), with T ranging from 0 to π. To calculate the finite

time behaviour of $C(\phi_4;\phi_3)$, a Mathematica program was used to calculate and normalize the eigenvectors for the numerical M and M^T, then using biorthogonality as described in section 2.4.4 and appendix C (C.1- C.4), these were used to obtain the values of r_μ and a_μ and consequently, using equation (3.61), reproduce and confirm the numerical form obtained for$M$ obtained earlier. M^n was then calculated using equation (3.64) for T ranging from 0 to π. The main ensemble size was chosen to be $m = 1000$ with sub-ensemble divisions for $\delta T = 0.01$. The $M(\alpha,\beta)$ 4 $\times$ 4 reproduced submatrix was then employed to calculate the finite time behaviour of $C(\varphi_4;\varphi_3)$ using equation (3.65) and a reasonable processing time was achieved. The program writes its intermediate steps and output to 6 different files relevant to one client and 5 labs based on their unique labindices . It was apparent afterwards that for problems involving many fermion modes (such as for the BEC/BCS crossover topic), it would be inevitable to make use of SUT's supercomputing facility.

D.1.3. Parallel Programming - C (ϕ_4; ϕ_3) program description

The first part of the $C(\phi_4;\phi_3)$ program for small $\delta T \ll 1$ (the generation of the L and K matrices and the matrix definitions of the $\delta\widetilde{\Omega}_a(\delta\widetilde{\Omega}_a{}^+)$ noise terms) was written using MatLab' s parallel processing capabilities on the SUT single processor with multiple cores. The program was then adapted to make use of multithreaded parallelism, and randomly generate the $\delta\widetilde{\Omega}_a(\delta\widetilde{\Omega}_a{}^+)$ noise terms sequences, calculate the Θ^-, Θ^+ products associated with the M 4 $\times$ 4 submatrix for each member of the ensemble within each of the 6 labs, and then finally calculate the various stochastic averages involved. The entire process was promising in terms of cutting down processing time and the unnecessary repetition of program runs which were associated with the analogous sequential program.

Overview of the C (ϕ_4; ϕ_3) program for small $\delta T \ll 1$ using the multi-threaded parallelism capability of MatLab:

- When starting the parallel processing pool associated with the SUT processor (Intel(R) Xeon(R) CPU E5-1650 v3, 3.50 GHz, 3501 Mhz, 6 Core(s), 12 Logical Processor(s)) which has 6 cores, 6 labs (a client and 5 workers) could be utilized, one for each core. The client's main goal is to processes the program common code which is used by all labs. The other five serving labs or workers process the pieces of code that depend on different data sets [57].
- The work between the client and the workers could be organized and synchronized using their unique identification numbers (lab indices).
- Using 'SPMD' (single program multiple data) blocks inside the source code, one can spread (or divide) the processing of the pieces of code or modules which use different data sets among the different workers or labs.
- The program opens 6 files (one for each lab) to display their processing results at the end of the program run. This in addition to a seventh file to display the results of processing the common data within the client.
- By default, the MatLab client and MatLab workers use different random number generators, even if the workers are part of a local cluster on the same machine with the client.The random generation algorithm for the client is by default (unless changed specifically) the Mersenne Twister algorithm ('twister'), (which is not quite suitable for some parallel processing purposes), the workers random generation algorithm is by default the 'Combined Multiple Recursive' ('CombRecursive' or 'mrg32k3a') algorithm [57].
- Since the MatLab command rng('shuffle') seeds the random number generator based on the current time, it should not be used to set the random number stream on different workers, to ensure the generation of independent streams. This is especially true when the command is sent to multiple workers simultaneously, such as inside a parfor, spmd, or a communicating job.
- Due to noticeable repetition in the random generated sequences of the client, a module was written to change its default Mersenne Twister based algorithm (Twister seed) to the combined recursive algorithm which is similar to that of the workers. Another module was written to ensure the non-repetition of the workers' random generation sequences (although the MatLab software design ensures that in most cases) which makes use of their lab indices.
- In the modified program, the main ensemble of size m is specified, the L, K matrices are built and the $\delta\widetilde{\Omega}_a$ and $\delta\widetilde{\Omega}_a{}^+$ matrices are defined respectively (common data to be used by all labs including the client). The processing is then transferred to the six available labs where different sets of $\delta\widetilde{\Omega}_a$, and $\delta\widetilde{\Omega}_a{}^+$ noise terms are randomly generated, where different values of δT are assigned to each lab. Consequently, each of the 6 labs processes analogous but different sets of data to produce different results (the stochastic averages) for the main

ensemble size specified. Within each lab the main ensemble size can be subdivided by taking its subsets, as was done before when using the sequential programs.

- For $m = 500$ and for one run of the program, the parallel pool processes data and produces results relevant to 6 different C points (one for each lab) depending on 6 different δT values assigned to each lab. In other words, for size $m = 500$ ensemble with its subdivisions, each run of the program involves 6 different calculations which are performed for the various stochastic averages involved within each lab, depending on different sets of randomly generated noise terms and different values of δT. Therefore, for $m = 500$, 6 multiplied by $500 = 3000$ records are processed for one run, 500 records for each lab.

D.1.4. Final remarks

The parallel pool processes 42 records in 30 min (actually 42 multiplied by $6 = 252$ records (or ensemble members' calculations) across the 6 parallel processing labs available). Consequently, and with a simple calculation (assuming the same number of records is processed in similar times), the program run takes approximately 5.9 hours to reach completion for a size $m = 500$ ensemble, after which data for different 6 C points for that ensemble size and its subdivisions can be gathered. This versus only one C point for a single run for that ensemble size as was the case with the old sequential program, for which the run took 3.5 hrs to reach completion. Therefore, the data needed for plotting the results for size $m = 500$ ensemble and its subdivisions can be gathered in just two program runs, rather than in 10 runs. As it turned out, the processing time is not exactly the same for the same number of records, and the program took about 3 hours and 40 minutes to process data for ensemble of size $m = 1000$ (6000 records are processed in that case.)

The parallel processing capability could also be used for calculating ensemble averages of the M matrix elements and this is expected to save processing time. For example, if each of 4 parallel processors calculates ensemble averages of $m = 100$ random generations of the M matrix elements and then average the outcomes for each processor, it should be equivalent to an ensemble average over $m = 400$ random generations, and achieved with the processing time for one processor.

ORCID iDs

B J Dalton https://orcid.org/0000-0002-1176-7528

References

[1] Abrikosov A A, Gorkov L P and Dzyaloshinski I E 1963 *Methods of Quantum Field Theory in Statistical Physics* (New York: Dover Publications)
[2] March N H, Young W H and Sampanthar S 1967 *The Many-Body Problem in Quantum Mechanics* (Cambridge: Cambridge University Press)
[3] Weimer H 2015 *Phys. Rev. Lett.* **114** 040402
[4] Frenkel J 1934 *Wave Mechanics* (Oxford: Oxford University Press)
[5] Feynman R P and Hibbs A R 1965 *Quantum Mechanics and Path Integrals* (New York: McGraw-Hill)
[6] Pitaevskii L and Stringari S 2003 *Bose–Einstein Condensation* (Oxford: Clarendon)
[7] Montina A and Castin Y 2006 *Phys. Rev.* A **73** 013618
[8] Drummond P D, Deuar P and Corney J F 2006 *Opt. Spectrosc.* **103** 7
[9] Drummond P D, Deuar P, Vaughan T G and Corney J F 2007 *J. Mod. Opt.* **54** 2499
[10] He Q-Y, Reid M D, Opanchuk B, Polkinghorne R, Rosales-Zárate L and Drummond P D 2012 *Frontiers of Physics* **7** 16
[11] Blakie P B, Bradley A S, Davis M J, Ballagh R J and Gardiner C W 2008 *Adv. Phys.* **57** 363
[12] Dalton B J, Jeffers J and Barnett S M 2014 *Phase Space Methods for Degenerate Quantum Gases* (Oxford: Oxford University Press)
[13] Schweber S S 1961 *Introduction to Relativistic Quantum Field Theory* (New York: Harper and Row)
[14] Berezin F A 1966 *The Method of Second Quantization* (New York: Academic)
[15] Drummond P D, Hu H and Liu X-J 2009 *J. Mod. Opt.* **56** 2076
[16] Hu H, Drummond P D and Liu X-J 2007 *Nat. Phys.* **3** 469
[17] Hu H, Liu X-J and Drummond P D 2006 *Europhys. Lett.* **74** 574
[18] King N, Polkinghorne R, Opanchuk B and Drummond P D 2019 *Phys Rev Letts* **122** 203604
[19] Fetter A L and Walecka J D 1971 *Quantum Theory of Many-Particle Systems* (New York: McGraw-Hill)
[20] Cahill K E and Glauber R J 1999 *Phys. Rev.* A **59** 1538
[21] Corney J F and Drummond P D 2006 *J. Phys.* A **39** 269
[22] Plimak L, Collett M J and Olsen M K 2001 *Phys. Rev* A **64** 063409
[23] Dalton B J, Garraway B M, Jeffers J and Barnett S M 2013 *Ann. Phys.* **334** 100
[24] Dalton B J, Jeffers J and Barnett S M 2016 *Ann. Phys.* **370** 12
Dalton B J, Jeffers J and Barnett S M 2019 *Ann. Phys* **406** 220 Corrigenda
[25] Polyakov E A 2016 *Phys. Rev.* A **94** 062104
[26] Dalton B J, Jeffers J and Barnett S M 2017 *Ann. Phys.* **377** 268
[27] Dalton B J, Jeffers J and Barnett S M 2017 *Fortschr. Phys.* **65** 1600038
[28] Matsubara T 1955 *Prog. Theor. Phys.* **14** 351
[29] Pitaevskii L and Stringari S 2003 *Bose–Einstein Condensation* (Oxford: Clarendon)

[30] Ketterle W and Zwierlein M W 2008 *Ultracold Fermi Gases, Proc. of International School of Physics "Enrico Fermi"* ed M Inguscio *et al* (Amsterdam: IOS Press)
[31] de Mello C A R 2008 *Phys. Today* **61(10)** 45
[32] Chin C 2016 *Nat. Sci Rev* **3** 168
[33] Chin C, Grimm R, Julienne P and Tiesinga E 2010 *Rev. Mod. Phys.* **82** 1225
[34] Duine R A and Stoof H T C 2004 *Phys. Rep.* **396** 115
[35] Parkins A S and Walls D F 1998 *Phys. Rep.* **303** 1
[36] Bardeen J, Cooper L N and Schrieffer J R 1957 *Phys. Rev.* **108** 1175
[37] London F and London H 1935 *Proc. of the Royal Society A: Mathematical, Physical and Engineering Sciences* **149** 71
[38] Popov V N 1966 *Zh. Eksp. Teor. Fiz.* **50** 1550
Popov V N 1968 *Sov. Phys. JETP* **23** 1034
[39] Keldysh L V and Kozlov A N 1968 *Zh. Eksp. Teor. Fiz.* **54** 978
Keldysh L V and Kozlov A N 1968 *Sov. Phys. JETP* **27** 521
[40] Eagles D M 1969 *Phys. Rev.* **186** 456
[41] Leggett A J 1980 *Proc. of the XVIth Karpacz Winter School of Theoretical Physics, Karpacz, Poland* (Berlin: Springer) p 13
[42] Heinzen D J, Wynar R, Drummond P D and Kheruntsyan K V 2000 *Phys. Rev. Lett.* **84** 5029
[43] Donley E A, Claussen N R, Thompson S T and Wieman C E 2002 *Nature* **417** 529
[44] Cornish S L, Claussen N R, Roberts J L, Cornell E A and Wieman C E 1979 *Phys. Rev. Lett.* **85** 1795
[45] Veeravalli G, Kuhnle E, Dyke P and Vale C J 2008 *Phys. Rev. Lett.* **101** 250403
[46] Sensarma R, Randeria M and Ho T-L 2006 *Phys. Rev. Lett.* **96** 090403
[47] Bulgac A, Forbes M M and Magierski P 2012 (*The BEC-BCS Crossover and the Unitary Fermi Gas* 836) ed W Zwerger (Berlin: Springer Lecture Notes in Physics) p 305
[48] Randeria M and Taylor E 2014 *Ann. Rev. Cond. Matt* **5** 209
[49] Torma P 2016 *Phys. Scr.* **91** 043006
[50] Zwerger W (ed) 2012 (*The BEC-BCS Crossover and the Unitary Fermi Gas* 836) (Berlin: Springer Lecture Notes in Physics)
[51] Nishida Y and Son D T 2007 *Phys. Rev.* A **75** 063617
[52] Nozieres P and Shmitt-Rink S 1985 *J. Low Temp. Phys.* **59** 195
[53] Prakash M, Prakash M, Venugopalan M R and Welke G 1993 *Phys. Rep.* **227** 321
[54] Gardiner C W 1983 *Handbook of Stochastic Methods for Physics, Chemistry and the Natural Sciences* (Berlin: Springer)
[55] Takagi T 1925 *Japan J. Math.* **1** 83
[56] Horn R A and Johnson C R 1985 *Matrix Analysis* (Cambridge: Cambridge University Press)
[57] MATLAB, Parallel Computing Toolbox 4 User's Guide R2013b, The MathWorks Inc. www.mathworks.com